5-1-2016

Bacteriophage virus-like particles as vaccine platforms : from heart disease to malaria

Erin Crossey

Erin Crossey
Candidate

Molecular Genetics and Microbiology
Department

This dissertation is approved, and it is acceptable in quality and form for publication:

Approved by the Dissertation Committee:

Bryce Chackerian, PhD, Chairperson

David Peabody, PhD

Brian Hjelle, MD

Michelle Ozbun, PhD

Bacteriophage virus-like particles as vaccine platforms:

From heart disease to malaria

by

Erin Crossey

B.A., Colorado College, 2007

DISSERTATION

Submitted in Partial Fulfillment of the
Requirements for the Degree of

Doctor of Philosophy

Biomedical Sciences

The University of New Mexico
Albuquerque, New Mexico

May 2016

Acknowledgements

I would like to thank all my lab-mates, past and present, for making this four years hard to leave behind. Julianne for help in every detail of every animal experiment, Kathryn for being a MATLAB and deep sequencing wizard, Mitch and John for advising me on my fantasy football draft picks and trades, Ebenezer for actual practical lab advice, Paul and Chris for scathing sarcastic commentary… Also you my committee members for light-handed but thoughtful guidance through this whole process! Especially, thanks Bryce for critical editing at deadlines (and beyond), and for building a great lab with great collaborators (here and elsewhere) and great projects.

Bacteriophage virus-like particles as vaccine platforms:
From heart disease to malaria

by Erin Crossey
B.A., Colorado College, 2007
PhD., Biomedical Sciences, University of New Mexico, 2016

Dissertation Abstract

Virus-like particles (VLPs) make excellent vaccines. They are non-infectious, often easy to produce in bacterial expression systems, and highly immunogenic. The latter feature is granted by the regularity of the capsid structure, which presents viral (or other) epitopes as dense, highly repetitive arrays that strongly stimulate B cells. VLPs can be used as the basis for vaccines targeting the virus from which they were derived, or they can be used as platforms to display practically any short peptide epitope in a multivalent format. Foreign peptides displayed on VLPs exhibit the same high immunogenicity as unmodified VLPs. Even self-antigens, normally subject to the mechanisms of B cell tolerance, are immunogenic when displayed at high density on the surface of VLPs. Several VLP-based vaccines that target heterologous foreign antigens derived from pathogens and self-antigens involved in disease are currently in clinical trials. As a powerful tool for vaccine development and discovery, we have applied VLP strategies in two different studies. We first generated a VLP vaccine targeting a self-antigen involved in cholesterol metabolism (PCSK9) that has exciting potential as a lipid-lowering agent. We next utilized VLPs in an affinity selection strategy to identify potential vaccine candidates that target a highly conserved malaria parasite target (AMA1) and have identified at least one VLP that elicits a relevant immune response. Through these studies we have expanded the applications for VLPs and further characterized methods for vaccine discovery for myriad targets in the future.

Table of Contents

List of Figures

Chapter 1

Chapter 2

Chapter 3

Chapter 4

List of Tables

Chapter 1: Virus-Like Particles in Vaccine Development

Virus-like particles as vaccines

Vaccines are one of the most influential health developments in human history. The ability to gain immune protection from pathogens without undergoing natural infection greatly reduces the burden of death, disease and disability worldwide. Vaccines are also typically safer and cheaper to produce than the therapeutic alternatives needed to manage most illnesses. In many cases, live-attenuated, inactivated or subunit vaccines have been sufficient to elicit protective immune responses. Live-attenuated and inactivated vaccines can be immunogenically potent, however the drawbacks of these types of vaccines are significant. Reversion of live-attenuated or improperly inactivated pathogens to virulent forms is a rare but serious possibility. In addition, inactivation processes are harsh and may destroy or alter the structures needed to elicit the desired immune response. While subunit vaccines are inert, and therefore safer, they are also less effective at eliciting potent immune responses. These vaccines often lack the dense repetitive structures that strongly stimulate B cells. Perhaps the most important drawback is that many pathogens are able to circumvent these types of strategies by rapid mutation of antigenic sites and shielding of critical or conserved regions. For pathogens with antigenically distinct subpopulations, vaccines composed of only one or several strains may fail to elicit protective immunity. In attempting to generate vaccines that can safely, potently and broadly neutralize pathogens such as these, new design strategies are therefore required.

Virus-like particles (VLPs) show promise in bridging these gaps. Like subunit vaccines, they are composed of inert protein and can be generated using recombinant techniques and bacterial expression systems. However, because VLPs are made from structural proteins that form capsids resembling the native viral structure, they are highly immunogenic similar to inactivated or live-attenuated vaccines. VLPs may target the virus from which the capsid protein is derived (Hepatitis B virus and Human Papillomavirus vaccines are two examples) [1, 2], or they may be used to display heterologous antigen [3-5]. Myriad techniques are available for VLP antigen display, and allow for diverse applications of this system. These include recombinant methods utilizing genetic insertion of heterologous sequences into surface-exposed sites of the VLP capsid, as well as chemical or enzymatic conjugation exploiting surface chemistries of the VLP. The flexibility of VLP display platforms for heterologous antigen display has important implications for rational vaccine design as well as empirical discovery of novel vaccine candidates.

Importantly, the underlying structure of the VLP grants a heterologously displayed antigen the same strong immunogenicity of the viral capsid itself [6]. This is possible because VLPs can display antigen in repetitive arrays with ideal spacing for cross-linking membrane-bound antibody on B cells and strongly signaling for their activation [7-9]. Therefore, VLP strategies may be used to develop vaccines targeting known structures that are immunosubdominant or weakly immunogenic in another context. Indeed, VLP display platforms have been used in humans to target both antigens derived from pathogens [10] as well as self-antigens [11]. The

potent immunogenicity of VLPs is especially illustrated by the ability to overcome B cell mechanisms of self-tolerance [12]. This feature extends the use of VLPs as vaccines that target pathogens to vaccines that elicit protective responses to self-targets implicated in chronic diseases. Diverse antigens specific to cancer, autoimmune disorders, CNS disease, allergy and cardiovascular disease have been identified and targeted by various therapeutic strategies [13-15]. The effective use of VLPs as vaccine platforms for both self and foreign antigen has several requirements, the first of which is identification of appropriate vaccine targets. This may be done by rational design, using sequence or structural characteristics of an antigen to guide design, or it can be done empirically using affinity selection to identify novel targets.

Rational vaccine design

Methods for identifying suitable antigen targets for VLP display. Epitopes represent the unique structures on antigens specifically recognized by the immune system. In the case of all T cell and some B cell epitopes, these structures are defined by the primary amino acid sequence encoded by the pathogen. Linear epitopes may be identified by the ability of the denatured protein target to bind a monoclonal antibody (mAb) of interest, and the specific sequence elucidated by screening antigen fragment libraries for binding to the mAb [16]. The existence of antibodies with desirable characteristics that bind these epitopes suggest that the cognate peptides derived from the antigen may be used in an effective epitope-based vaccine [15]. In this way (as well as in the affinity selection strategies that will be discussed

below) mAbs that have the ability to bind and neutralize pathogens or self-antigen can contribute to vaccine design.

Recent advances in structural biology have also paved the way for rational vaccine design [17, 18]. Characterization of the protein regions important for interactions that occur during infection is one method for identifying relevant target epitopes for example. The crystallographic data available in the Protein Database (for nearly 100,000 structures) allow us to distinguish surface-exposed regions of interest, especially when complexes of the relevant binding partners have been visualized [19, 20]. Other means of identifying interaction-critical epitopes are by deletion or mutagenesis studies, which elucidate necessary domains or residues by assessing the binding properties of mutant proteins [21]. In addition, for pathogens that undergo antigenic variation, identifying specific neutralizing epitopes can be aided by the mapping of polymorphic residues. This type of study indicates regions of high antigenic variation that should be avoided or optimized in vaccine design [22]. Each of these methods can be used to reveal epitopes of interest that, when displayed as peptides on VLPs, may become highly immunogenic targeted vaccines.

Chemical conjugation. Once an epitope target has been identified, several mechanisms for VLP display are available. The first is chemical conjugation, which utilizes the surface chemistry of the VLP to attach peptides. For example, the presence of surface-exposed primary amino groups can be used to attach peptides that have been engineered with a terminal cysteine residue, using the bifunctional cross-linker succinimidyl 6-[(β-maleimidopropionamido)hexanoate] (SMPH). This

method is typically used in conjunction with the bacteriophage Qβ that has surface-exposed lysine residues, and has been used in several preliminary human vaccine trials that target self-antigens [23, 24]. This technique generally displays peptide in a conformationally unconstrained manner, but cyclized peptides may be engineered and used in chemical conjugation as well.

Sortase enzyme-mediated conjugation. A second recently developed (in our lab) method for peptide display on VLPs is enzymatic conjugation using the bacteria-derived sortase enzyme for sequence-targeted attachment. This strategy has been described recently for use in M13 bacteriophage display [25], as well as in the development of a *B. anthracis* conjugate vaccine [26]. Sortase is a transpeptidase derived from *S. aureus* that naturally functions in anchoring proteins to the bacterial cell wall. A 'sorting motif' is first recognized by the enzyme; the pentapeptide is LPXTG for *S. aureus*-derived sortase, but other sequences are recognized by other sortases [27]. A catalytic cysteine residue on the enzyme is then used to cleave the peptide bond between the threonine and glycine residues. Sortase accepts the N-terminus of an oligoglycine nucleophile, which results in the formation of a new peptide bond. Calcium ions stabilize substrate binding to sortase and increase the activity of the enzyme ~8 fold [28]. The main advantage of this form of conjugation is more precise site-specificity of attachment than can be achieved by chemical conjugation methods, and also the ability to attach peptides with internal cysteine residues. To apply this strategy to sortase-mediated VLP modification, we have taken two approaches.

First, a bacteriophage MS2 coat protein was engineered to encode an N-terminal pentaglycine sequence, and a FLAG peptide was constructed with a C-terminal LPETG sequence motif. A pET22 expression vector that was developed in the lab of Dr. Hidde Ploegh (MIT) [and was a gift from Dr. Anette Schneemann (Scripps)], encoding a hexa-histadine tagged sortase enzyme from *S. aureus,* was used to express the enzyme in transformed BL21(DE3) cells, using ampicillin to restrict growth. Crude cell lysates were purified by Ni-NTA resin (ThermoScientific) affinity chromatography. Pooled elution fractions containing sortase (as verified by denaturing polyacrylamide gel electrophoresis) were dialyzed against a 20mM Tris pH8, 150mM NaCl, 10% glycerol solution. Conjugation reactions contained 50uM peptide, 200nM recombinant 5G-MS2 VLPs and between 0-100uM[**] sortase enzyme [29], were diluted to 10-100uL in TBS with 10mM $CaCl_2$ and incubated at 37°C for 3 hours. The N-termini FLAG-conjugated MS2 VLPs were then analyzed on a denaturing polyacrylamide gel and blotted with both a FLAG mAb and anti-MS2 polyclonal sera in a Western blot (Figure 1.1). We observed the presence of a ~28kDa FLAG-conjugated MS2 band at each of the concentrations of sortase tested, and no band in the negative reaction lane that underwent the same treatment without sortase enzyme in the reaction. A slight electrophoretic mobility shift was observed on an agarose gel between conjugated and unconjugated 5G MS2 VLPs, indicating the likely presence of FLAG-conjugated VLPs (a similar gel could be run longer to better discriminate this).

[**] The need for a high concentration of sortase is that the deprotonated form of cysteine is required for catalysis, and at physiologic pH ionized forms are at equilibrium with neutral forms, resulting in only ~0.06% of the enzyme being catalytically competent at a given time.

Second, a bacteriophage MS2 coat protein was engineered to encode an AB loop $(NNS)_2$LPETG$(NNS)_2$ sequence, and a FLAG peptide was constructed with an N-terminal pentaglycine sequence motif. The AB loop MS2 construct was randomized at each of the flanking 2 amino acid positions for the purpose of screening clones first for correctly folded coat protein and subsequently for optimal sortase compatibility. It was expected that in this scenario sortase conjugation would result in coat protein dimer cleavage at the AB loop, and result in smaller bands than observed previously. Coat protein folding assays were performed by Dr. Dave Peabody, using translational repression of replicase-β-galactosidase fusion protein expressed from one plasmid to assess the correct folding of recombinant MS2 coat protein expressed from a second plasmid. Co-transformed CSH41 cells were streaked on X-gal-containing plates, with white (*vs*. blue) colonies representing those in which translation of β-galactosidase has been repressed by correctly folded coat protein [30]. Reactions were performed exactly as before, and AB loop FLAG-conjugated MS2 VLPs were analyzed on a denaturing polyacrylamide gel and blotted with a FLAG mAb in a Western blot (Figure 2.1). We observed the presence of a small ~14kDa FLAG-reactive band in 6 of the 24 MS2 AB loop variants tested (only a subset are shown), and no band in the negative reaction lane that underwent the same treatment without sortase enzyme in the reaction. We observed similarly sized bands in reactions containing pure or crude VLP preps (data not shown). However, further studies need to be performed by blotting for MS2 to detect the ratio of unconjugated (28kDa dimer; no FLAG band) *vs*. conjugated coat protein (sortase-cleaved dimer; 14kDa FLAG band) in these reactions, as the efficiency

seems significantly decreased compared to the first sortase conjugation scenario using pentaglycine N-terminus MS2. Also, no shift was observed on an agarose gel comparing unconjugated to sortase FLAG-conjugated VLPs (data not shown), which likely reflects that the low level of cleaved/conjugated coat protein does not form VLPs (a significant downward shift is expected in FLAG-VLPs compared to wild type).

These studies indicate that a) that recombinant MS2 VLPs can be conjugated by sortase, b) sequence variation around the sortase recognition sequence in the AB loop affects the efficiency of enzyme-mediated conjugation, and c) the high specificity of sortase-targeting will likely allow the use of crude preparations of VLPs rather than purified VLPs. We currently have more confidence in the 5G-MS2/peptide-LPETG scenario of sortase-mediated conjugation, but further development of both mechanisms would be useful.

Genetic insertion of target sequences. The third method for heterologous antigen display on VLPs was touched on briefly in the previous section discussing recombinant VLPs that encoded the sortase recognition motifs. More specifically however, we have developed 2 flexible display platforms using MS2 and PP7 bacteriophage VLPs, which are amenable to recombinant heterologous antigen display at several surface-exposed sites of the coat proteins. The benefits of recombinant VLPs are the guaranteed regularity of display of the antigen in the same conformation (provided coat protein folding or VLP formation is not perturbed by the insert), as well as the production advantages over chemical and

sortase-mediated conjugation. The importance of choosing a site for insertion lies in VLP-surface exposure and density of the site as well as coat protein folding tolerance to insertion (i.e. correct folding despite foreign sequence). We have used both the coat protein N-terminus as a site for unconstrained peptide display (Figure 1.1A) and a flexible AB loop for constrained display (Figure 1.2A) for peptide insertions of individual targets [31].

In addition, our lab has previously shown that the genetic fusion of two copies of coat protein in a single-chain dimer format, and the use of only the downstream copy for insertion of heterologous sequences into a surface-exposed AB loop, results in coat protein that is highly tolerant to diverse inserts. Approximately 96% of 6mers were tolerated in the blue/white screen of coat protein folding described above, and 94% of 8mers and 92% of 10mers [3, 32]. Almost equally high percentages of those insertions allowed VLP formation; of the ~20 white colonies that were screened for each insert length, 100% of 6mers, 87% of 8mers and 80% of 10mers were tolerated by agarose gel and Western blot screen for VLP formation. VLP encapsidation of insert-containing RNA was also confirmed, by agarose gel and Northern blot. The existence of the highly tolerant AB loop site for peptide insertion has facilitated the creation of highly diverse random peptide libraries of 6, 7, 8 and 10mer displayed on MS2 VLPs ($>10^8$). Random peptide display on VLPs can be a potent tool for vaccine discovery by allowing the identification of novel epitope-based vaccines by affinity selection strategies. In utilizing a highly immunogenic platform for display (VLPs), the epitope presentation context is preserved from discovery to vaccination. This is critical for vaccines that target complex epitopes.

Affinity selection for vaccine discovery

In contrast to the linear B cell epitopes that are more amenable to rational design, many B cell epitopes exist only in the tertiary structure of an antigen, and are formed by discontinuous amino acid sequences brought in close proximity by protein folding. The targeting of discontinuous and complex epitopes with vaccines has been limited in the past by the inability to immunogenically present individual epitope-like structures that elicit the appropriate immune response (i.e. one that recognizes the epitope on the native protein) [33, 34]. The first description of a mimotope, or a peptide that mimics the structure of an epitope, identified peptides that bound an antibody recognizing a discontinuous epitope [35]. Since then, screening of filamentous phage-displayed libraries of peptides has been instrumental in identifying mimotopes of many epitopes of interest in vaccine design [36-38]. By using mAbs with desirable characteristics to screen these libraries for binding, peptides with the potential to elicit a similar antibody response *in vivo* may be isolated. Although phage display is powerful in identification of peptide mimics, it is a poorly immunogenic platform. The need to transfer the peptide to another display context frequently results in a loss of immunologic mimicry, and the failure to elicit the intended immune response. As an alternative, VLPs derived from bacteriophage have many of the characteristics of filamentous phage used in traditional affinity selection strategies, and may represent a novel platform for affinity selection-based vaccine discovery.

Like live phages, VLPs retain the intrinsic ability to encapsidate their encoding genomic material. In the case of VLPs made from recombinantly expressed bacteriophage coat proteins, this is simply the plasmid-derived mRNA. In heterologous antigen display utilizing genetic insertion of sequences into the coat protein, the encapsidated material includes the insert sequence and establishes a genotype/phenotype link necessary for identification and PCR-based amplification of selectants in iterative rounds of affinity selection [39].

We have shown that we can create diverse libraries of peptide-displaying VLPs (discussed in depth above), and we have therefore applied them in an affinity selection strategy using a malaria parasite-neutralizing mAb that recognizes a conformational epitope. Using deep sequencing to critically assess the selectants and aid in choosing vaccine candidates, we have a broad snapshot of a selection using our VLP strategy and have identified at least one malaria-targeted VLP vaccine of interest (Chapter 3). Also, in order to explore the design of a rational vaccine target using all of the VLP platforms at our disposal, we have chosen a self-antigen involved in lipid metabolism to target. We have compared each of the platforms and found at least one vaccine that significantly lowered cholesterol (Chapter 2).

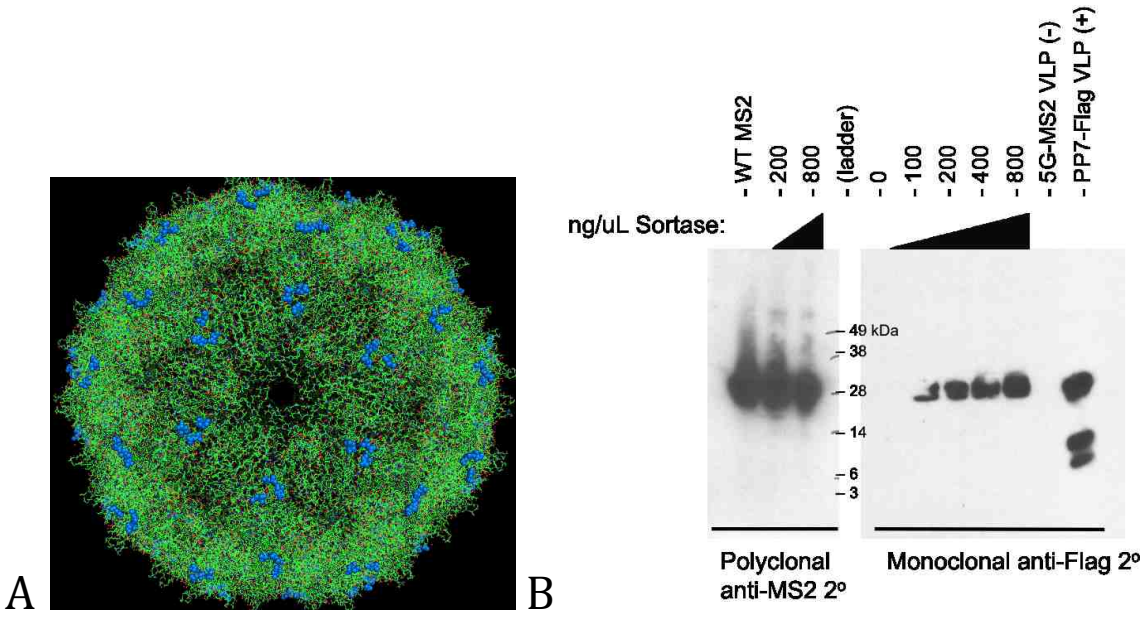

Figure 1.1. MS2 N-terminal site-directed sortase conjugation of FLAG peptide. The crystal structure of the bacteriophage MS2 VLP is shown, with N-termini of MS2 coat protein highlighted in blue (A). This was the site of LPETG motif-directed sortase conjugation used to generate the first version of FLAG-tagged VLPs. Also shown is a Western blot using anti-MS2 polyclonal rabbit sera (left) and anti-FLAG monoclonal antibody (right) to detect conjugated VLPs (B). The single-chain dimer version of coat protein runs at ~28kDa. Sortase-mediated conjugation of FLAG peptide was seen at each concentration of sortase used in the reaction mixture. Controls include a no-sortase reaction mixture ('0'), wild-type MS2 VLPs (left), and a recombinant FLAG-expressing PP7 VLP (right). An agarose gel was also run, and a slight shift was seen between unconjugated and sortase-mediated FLAG-conjugated 5G-MS2 VLPs (C). The MS2 image in panel A was generated using the coordinates provided by the VIPER database using the program PyMOL.

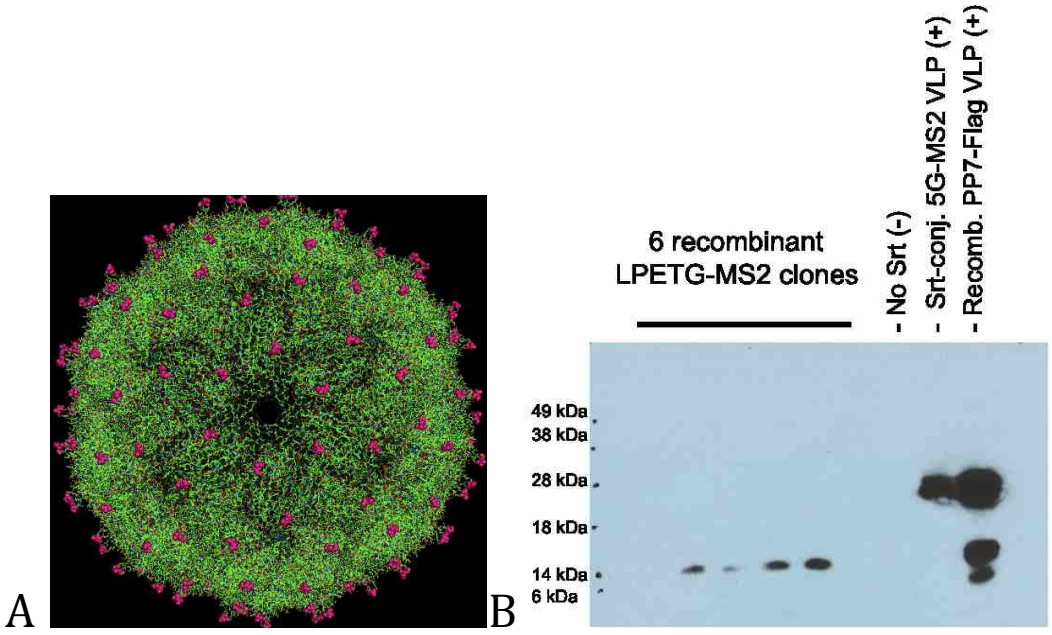

Figure 1.2. MS2 AB-loop site-directed sortase conjugation of FLAG peptide. The crystal structure of the bacteriophage MS2 VLP is shown, with surface exposed AB-loops of MS2 coat protein highlighted in magenta (A). This was the site of LPETG motif-directed sortase conjugation used to generate a second version of FLAG-tagged VLPs. Also shown is a Western blot using anti-FLAG monoclonal antibody to detect conjugated VLPs (B). The single-chain dimer coat proteins (which normally run at 28kDa) have been cleaved by sortase at the AB loop and can be identified as ~14kDa bands. Three out of six clones tested had apparent sortase-mediated conjugation of FLAG peptide. Controls include a no-sortase reaction mixture, FLAG-conjugated N-terminal glycine MS2 VLPs (described in Figure 1), and a recombinant FLAG-expressing PP7 VLP. The MS2 image in panel A was generated using the coordinates provided by the VIPER database using the program PyMOL.

Chapter 2: Generation of a Cholesterol-Lowering Vaccine that Targets PCSK9

Abstract

Proprotein convertase subtilisin/kexin type 9 (PCSK9) is a secretory protease involved in cholesterol homeostasis by enhancing endosomal and lysosomal degradation of cell surface low-density lipoprotein receptors (LDL-R). While mutations causing increased activity of PCSK9 have been found to be associated with hypercholesterolemia, atherosclerosis and early coronary heart disease (CHD), healthy patients have also been identified with loss-of-function PCSK9 mutations, which exhibit a hypocholesterolemia phenotype and up to 88% decreased risk of CHD. These observations indicate that PCSK9 is an attractive target for the purpose of lowering circulating LDL-cholesterol (LDL-C), and therefore decreasing the potential for CHD and atherosclerosis. In this study, we generated a PCSK9-targeting vaccine by conjugating a human-PCSK9-derived peptide to Qβ bacteriophage virus-like particles (VLPs). Mice vaccinated with PCSK9-conjugated Qβ developed high titer anti-peptide and anti–hPCSK9 IgG responses. Total cholesterol, free cholesterol, phospholipid and triglyceride levels decreased significantly in the PCSK9-Qβ vaccinated group. Thus, a PCSK9-targeted vaccine may be an effective therapeutic for lowering cholesterol. In addition, because statins are somewhat self-limiting in efficacy due to up-regulation of PCSK9 along with LDL-R, they could be used in conjunction with PCSK9-targeting therapeutics such as this vaccine,

potentially increasing efficacy and decreasing cost and dosing in hypercholesterolemia therapies.

Introduction

Atherosclerosis is the underlying cause of CHD, and has many risk factors including smoking, poor diet, insufficient exercise, stress, hypertension, diabetes and dyslipidemias. This last risk factor is most commonly characterized by an increase in very low-density lipoprotein (VLDL) and low-density lipoprotein (LDL) particles, and concomitant elevation of serum LDL-C. Autosomal dominant hypercholesterolemia (ADH) is classically associated with mutations in the genes encoding the LDL-R and its ligand apolipoprotein B (ApoB), however proprotein convertase subtilisin/kexin type 9 (PCSK9) is another important regulatory protein involved in the cellular uptake of LDL [40]. The presence of increased serum LDL-C levels (>300 mg/dL) and premature CHD in human populations with gain-of-function mutations in PCSK9 strongly supports its important role in regulating LDL-C [41]. In addition, human subjects that carry loss-of-function PCSK9 mutations have been identified in several populations and exhibit 15-25% decrease in mean serum LDL-C as well as 47-88% reduction in the incidence of CHD over a 15-year period [42]. Several subjects have been identified that carry compound heterozygote loss-of-function mutations, exhibiting serum LDL-C of <20 mg/dL, and appear healthy despite having no detectible circulating PCSK9 [43]. The existence of these mutations and their associated phenotypes make PCSK9 an attractive

therapeutic target for lowering LDL-C and potentially decreasing the incidence of CHD.

PCSK9 is a serine protease composed of a signal peptide, prodomain, catalytic domain, and C-terminal histidine-rich domain [44]. Autocatalytic cleavage of the signal peptide in the endoplasmic reticulum is followed by several post-translational modifications before the soluble protein is secreted from the cell, after which it is no longer catalytically active [45]. It has been established that PCSK9 binds directly to and promotes the internalization of LDL-R on the surface of cells, most notably in the liver, increasing the circulating amount of LDL-C by preventing its uptake [20, 46]. Normally, circulating ApoB and ApoE-containing lipoprotein particles (i.e. LDL and intermediate-density lipoproteins (IDL), respectively) are endocytosed upon LDL-R binding, followed by lysosomal catabolism of particles and recycling of LDL-R to the cell surface; the presence of PCSK9 inhibits this process in an affinity-dependent manner, increasing the amount of circulating lipoprotein particles capable of depositing in vessels and causing downstream pathology, including atherosclerosis and CHD [45].

Statins are currently the best available therapy for CHD, but unfortunately this therapy increases circulating levels of PCSK9 by >30% in humans as compared to placebo, making them somewhat self-limiting in their ability to reduce LDL-C [9-11]. This likely occurs because a transcription factor that is indirectly upregulated by statins (sterol regulatory element-binding protein-2, SREBP-2) activates both *Ldlr* and *Pcsk9* genes [47]. Indeed, statins are much more effective when there is a deficit

of PCSK9, as shown in PCSK9 knockout mice [48]. Therefore, especially in vulnerable populations such as those resistant to statin therapy, PCSK9-targeted therapeutics will be incredibly valuable in preventing and treating CHD.

Disruption of the interaction between PCSK9 and LDL-R has recently been the subject of many exciting studies, especially by the use of PCSK9-specific monoclonal antibodies (mAbs). Successful preliminary mouse and primate studies have even translated in several cases to successful late-phase human trials [15, 49, 50]. Although MAb therapeutics have been used for pathologies such as cancer, transplant rejection, autoimmune and infectious diseases, they remain expensive to manufacture and require lifelong therapy, as the terminal half-life of infused humanized mAbs is at best ~1 month, and often less [51, 52]. Other drawbacks are the complications that may arise if the mAb generates aberrantly immunogenic reactions to the therapeutic itself, or the therapy elicits a dangerous 'cytokine storm' reaction [53-55]. One alternative to mAb therapies is to develop a vaccine that elicits a similarly targeted and specific response as that of the mAb. In the case of PCSK9, structural data is available for the protein that aids the rational design of peptide-based vaccines that target the LDL-R-binding regions of PCSK9 in particular [20, 44]. While immune tolerance mechanisms normally preclude generation of an immune response to self-antigen, several studies have shown that the context of antigen, for example arraying peptide on virus-like particle (VLP) surfaces, can overcome this barrier [12, 56-59].

VLP-based vaccines are a reasonable strategy for stimulating B cell responses due to the ordered, multivalent organization of antigen presented on their surface. A repetitive array of antigen is capable of cross-linking B cell surface immunoglobulin (Ig) molecules and inducing strong intracellular signaling that ultimately results in increased antibody secretion and up-regulation of T cell co-stimulatory molecules. The ability of VLPs to stimulate self-reactive, anergic B cells has been shown, supporting the use of this platform in generating an autoantibody response should a suitable self-target be identified as a candidate for active immunotherapy [8, 11]. Bacteriophage VLPs in particular, displaying heterologous peptide antigen, have been used in the past to successfully overcome B cell tolerance in both animal models and clinical trials in humans [29, 30].

In this study we have used VLPs derived from the structural coat proteins of several bacteriophages to display various PCSK9 peptides, in order to generate targeted Ab responses that have clinically relevant downstream effects such as lowering serum cholesterol, phospholipid and triglycerides, by decreasing and/or neutralizing extracellular PCSK9 and increasing liver LDL-R. We identified regions of interest on the protein, investigated different VLP platforms and methods of display for the PCSK9-derived peptides, and then tested the ability of candidate vaccines to modulate plasma lipids and PCSK9 in a mouse model.

Materials and Methods

Conjugation of peptide to Qβ VLPs. Qβ VLPs were generated by transfecting C41(DE3) *E. coli* cells (Lucigen) with an expression vector containing the Qβ coat

protein. Transformed cells were grown at 37°C to an OD_{600} of 0.6-0.8 prior to induction with 0.5mM IPTG. The culture was allowed to grow an additional 5 hours at 37°C, after which cells were pelleted by centrifugation and frozen at -20°C overnight. VLPs were purified from the soluble fraction of cell lysates by FPLC. PCSK9 peptides (listed in Table 2.1; synthesized by GenScript) included a C-terminal cysteine residue preceded by a 2-glycine-spacer sequence, to allow conjugation to VLPs using the bifunctional cross-linker succinimidyl 6-[(β-maleimidopropionamido)hexanoate] (SMPH; ThermoScientific). First, Qβ VLPs were incubated with SMPH dissolved in DMSO at a molar ratio of 10:1 (SMPH:VLP, diluted in PBS), for 2 hours at room temperature. VLPs were buffer-exchanged into PBS and excess SMPH linker was removed from the VLP prep using the Amicon-Ultra-4 centrifugal filter columns with a 100kDa MW-cutoff (Millipore). Peptide was then added to the VLP prep at a molar ratio of 10:1 (peptide:VLP, diluted in PBS), and incubated overnight at 4°C. VLPs were again buffer-exchanged into PBS and excess peptide was removed from the VLP prep using Amicon 100kDa MW-cutoff columns (Millipore). Conjugation efficiency and concentration of final VLP-peptide prep was assessed by denaturing polyacrylamide gel electrophoresis.

Generation of recombinant MS2 and PP7 VLPs. Recombinant VLPs were generated by transfecting C41(DE3) *E. coli* cells with an expression vector containing the MS2 or PP7 coat protein in a single-chain dimer format, as previously described [4, 32, 39]. Each clone included a PCSK9 peptide sequence of interest in either the amino-terminus position or a surface-exposed AB-loop position. PCSK9 sequences

representing amino acids 68-76, 153-163, 188-200, 208-222 and 368-381 were cloned into plasmid pDSP62 (MS2) or pDSP7k (PP7) by PCR, using the forward primers listed in Table 2.1. To aid in cloning, forward primers for MS2 N-terminal insertion included a unique NcoI site, and forward primers for PP7 AB-loop insertion included a unique KpnI site. In all cases reverse primer E3.2 (5' CGGGCTTTGTTAGCAGCCGG 3') was used, which anneals downstream of a unique BamHI site; PCR fragments were cloned using either NcoI/BamHI or KpnI/BamHI sites into the pDSP62 or pDSP7k expression plasmids, respectively. All resulting constructs were sequenced to verify correct location and sequence of PCSK9 insert. Recombinant MS2 and PP7 VLPs were expressed and purified as described above for Qβ VLPs. Formed VLPs containing RNA were detected by ethidium bromide (Invitrogen) on a 1% agarose gel, and quantified by denaturing polyacrylamide gel electrophoresis.

Immunizations. For all experiments except the Western diet experiment, VLP immunogenicity was determined by immunizing groups of 4-5 male Balb/C mice intramuscularly three times at 2-week intervals, with 5μg of FPLC-purified PCSK9 peptide-conjugated Qβ VLPs, recombinant MS2 or PP7 VLPs, or as negative controls, wild-type Qβ, MS2 or PP7 VLPs (50uL total volume, with 50% incomplete Freund's adjuvant). In the case where a mixture of VLPs was used to immunize mice, 2.5ug of 4 separately purified preparations of VLPs were combined for a total of 10ug per immunization, and 3 immunizations at 2-week intervals were given as described. In the Western diet experiment, the mice used were C57BL/6 mice, divided into two groups of three, and the immunization protocol used was identical to that described

previously. The sole vaccine used in this model was the PCSK9 (207-223)-Qβ vaccine. All animal studies were performed in accordance with guidelines of the NIH and UNM Animal Care and Use Committee (protocol 12-100827-HSC).

Characterization of antibody responses. Plasma was collected in heparinized pipettes and tubes prior to first immunization and 2-weeks following the third immunization, by intraocular bleed or cardiac bleed respectively, while animals were anesthetized. Peptide-specific IgG titers were determined by end-point dilution ELISA using cognate peptide as the immobilized target as follows (washing between each step four times with PBS using a multi-channel plate washer).

To determine peptide-specific IgG titers elicited by vaccine candidates, ELISA plates were incubated with streptavidin (Invitrogen) at a concentration of 500ng/well in PBS for 2 hours at 37°C. SMPH (Thermo Scientific) was added to wells at 1ug/well in PBS and incubated for 2 hours at room temperature. Individual peptides corresponding to the Qβ-conjugated peptides in Table 2.1 were added to the wells at 1ug/well in PBS and incubated overnight at 4°C. Plates were blocked with 0.5% milk in PBS for 2 hours at room temperature, and dilutions of mouse plasma were added to each well and incubated for 2.5 hours at room temperature. The wells were probed with horseradish peroxidase (HRP)-conjugated goat anti-mouse-IgG secondary antibody (Jackson ImmunoResearch) at a dilution of 1:5,000. 50uL of TMB substrate (ThermoScientific) was used to develop plates, followed by neutralization of developer within 30 minutes with an equal volume of 1% HCl solution. Reactivity of sera for target peptide was determined by measuring mean

optical density (OD) values at 450nm. Wells with twice the mean OD value of background were considered to be positive.

To determine PCSK9-reactive IgG titers elicited by vaccine candidates, ELISA plates were incubated with recombinant human PCSK9 protein (R&D Systems) at a concentration of 500ng/well in PBS overnight at 4°C. Plates were then blocked and treated exactly as above for peptide ELISAs, with the exception that end-point dilutions were generated from pooled plasma samples from groups of mice that received the same vaccine.

Plasma lipid quantification. Plasma total cholesterol, free cholesterol, phospholipid and triglycerides were measured using a ChemWell instrument and Roche reagents at the Lipoprotein Metabolism Section of the NHLBI/NIH.

Plasma PCSK9 quantification. Plasma PCSK9 was detected by a mouse PCSK9 ELISA kit (R&D Systems, MPC900), as per manufacturer instructions. Plasma PCSK9 was quantified by comparing experimental sera samples diluted 200-fold to an internal standard curve, using Prism 5 software to perform non-linear regression analysis (R^2 = 98.9-99.9%). PCSK9 was quantified in this way both before and after removal of immunoglobulin using Protein G-coated magnetic beads (Life Technologies, 10004D), as per manufacturer instructions. Briefly, plasma samples diluted 1:200 were split into equivalent volumes, then either a) incubated for 10 minutes rocking at room temperature with magnetic Protein G beads or b) set aside at room temperature. The Protein G beads were isolated using a magnet, and the Ig-cleared

supernatant (a) was then used directly in the PCSK9 ELISA kit, alongside the non-Protein G-treated plasma sample (b).

Statistical analysis. Single comparisons were made with unpaired, two-tailed t-tests using SPSS Statistics software. When Levene's test for equality of variances was found to be a significant factor, the p-values were derived from t-tests performed without equal variances assumed.

Results

Generation of VLPs displaying PCSK9 peptides. In this study, we have developed vaccines targeting PCSK9 by displaying human PCSK9-derived short peptides (9-16 amino acids) in a highly immunogenic format on the surface of bacteriophage VLPs. Peptides were chosen based on the literature [15] and the crystal structure of PCSK9 (Figure 2.1), and were arrayed on three types of VLPs (Figure 2.2). The two methods used to display peptide included chemical conjugation of synthetic PCSK9 peptides to the VLP surface or by engineering PCSK9-displaying recombinant VLPs. Chemical conjugations were performed using a bifunctional cross-linker (SMPH) with amine- and sulfhydryl-reactive arms. PCSK9 peptides were synthesized with terminal cysteine residues and were conjugated to primary amine on the surface of pre-formed Qβ VLPs. As shown in Figure 2.3a, this technique results in high-valency display of peptide on the surface of the VLP. We estimate that ~270 copies of the PCSK9 peptide are displayed per VLP.

Recombinant VLPs were constructed by genetically inserting sequences representing PCSK9-derived peptides at the N-terminus or the downstream AB-loop

of a single-chain dimer version of the MS2 or PP7 bacteriophage coat protein. We have previously shown that single-chain dimer versions of MS2 and PP7 coat protein are tolerant of insertion of diverse heterologous sequences without interfering with the ability of the recombinant protein to fold and self-assemble into VLPs [4, 32]. Peptides were displayed either at the N-terminus of the MS2 coat protein (Figure 2.2), which results in unconstrained display of peptide, or at a surface-exposed and constrained loop (the AB-loop) on PP7 coat protein. In each case, 90 copies of the PCSK9 peptide are displayed on each VLP. Upon expression, recombinant VLPs were purified and then characterized by agarose gel electrophoresis. Intact VLPs migrate through the gel due to their overall electrophoretic charge and can be visualized using ethidium bromide by virtue of the RNA that is encapsidated by the particles (Figure 2.3B). Thus, this assay can be used to demonstrate the production of intact VLPs, and to measure charge differences that are conferred by the peptide epitopes that are displayed on the surface of the VLPs.

Using these techniques, we constructed three PCSK9-displaying Qβ VLPs via the conjugation technique, and seven recombinant MS2 and PP7 VLPs displaying PCSK9 peptides (Table 2.1).

High peptide-specific and PCSK9-reactive IgG titers achieved with immunization. In order to compare our vaccine candidates, we immunized groups of 4-5 Balb/C mice with PCSK9-conjugated Qβ VLPs, recombinant PCSK9-MS2/PP7 VLPs, or, as a control, wild-type VLPs. Mice immunized with PCSK9-VLPs generated high-titer

antibody responses against PCSK9 (Figure 2.4). Several peptides were displayed on both Qβ and MS2 or MS2 and PP7, allowing a head-on comparison of these platforms. The chemical conjugation technique elicited 10-100 fold higher IgG titers for the $PCSK9_{153-163}$ peptide and PCSK9-specific responses, suggesting that peptide valency affects the magnitude of the antibody response (Figure 2.5). However, similar peptide titers were elicited with the $PCSK9_{207-223}$ vaccines displayed on both Qβ and MS2 (data not shown), so this effect may be peptide/target specific. We also gave one group of mice a mixed vaccine of 3 Qβ-based vaccines while also testing each separately. The mixed immunization consisted of 2.5ug of each of three VLPs. High peptide and PCSK9 titers were elicited by the individual Qβ vaccines, and the mixed Qβ vaccine elicited comparably high titers of IgG responses against each component peptide represented in the vaccine, as well as PCSK9 (Figure 2.6).

Decreased plasma lipid levels were achieved with immunization. In order to assess the functional effect of immunization against the various PCSK9 epitopes, we quantified circulating lipid levels in vaccinated mice. We measured triglycerides, total and free cholesterol, and phospholipids. We found that functional outcome varied between different epitopes targeted and vaccine platforms used (Figure 2.7). The most consistent lipid decreases were seen in the group of mice given the Qβ-$PCSK9_{207-223}$ vaccine, with relative plasma levels of triglycerides, total and free cholesterol, and phospholipids all significantly lower compared to controls after three immunizations ($p < 0.05$). Comparing relative change in lipid levels in the $PCSK9_{207-223}$-immunized mice compared to control mice, triglycerides were

decreased by 66.8%, free cholesterol by 53.7%, total cholesterol by 50.0% and phospholipid by 9.5%. Although several other vaccine candidates produced significant decreases in individual lipid parameters, we decided to focus on the most promising vaccine candidate (Qβ-PCSK9$_{207-223}$). In total we vaccinated 20 mice with this vaccine (Figure 2.8) and found that Qβ-PCSK9$_{207-223}$ consistently lowered circulating lipids relative to mice immunized with control VLPs ($p < 0.001$). Specifically, triglycerides were decreased by 50.8% in PCSK9$_{207-223}$-immunized mice compared to control mice, free cholesterol by 38.3%, total cholesterol by 27.5% and phospholipid by 27.3%.

Decreased plasma triglyceride levels in immunized mice fed a Western diet. We next assessed the effect of immunization against PCSK9 in a high-fat diet model. We quantified circulating lipid levels in C57BL/6 mice given high levels of dietary saturated fat, cholesterol and cholic acid (i.e. a Western diet), prior to and after immunization with the Qβ-PCSK9$_{207-223}$ vaccine. Although anti-PCSK9 antibody levels were approximately 10-fold lower in C57BL/6 mice compared to Balb/C mice, these titers have remained durable for 6 months, and vaccination resulted in a significant decrease in plasma levels of triglycerides compared to controls ($p < 0.05$) (Figure 2.9). Total cholesterol, free cholesterol and phospholipids were not significantly different between groups after immunization.

Presence of Ig-bound PCSK9 in plasma of immunized mice. To determine the effects of vaccination on plasma PCSK9 levels, we quantified protein in preimmune plasma plasma as well as plasma obtained after three immunizations of Balb/C mice.

Plasma PCSK9 was found to be comparable in both groups at the initial time point, but significantly higher at the final time point in plasma from the experimental group as compared to control vaccinated animals (Figure 2.10). However, upon removal of IgG from the plasma using a single treatment with magnetic Protein G beads (which bind the constant region of IgG and allow clearance of IgG-bound antigen from plasma samples), there was a significant decrease in the amount of PCSK9 detected in experimental samples, but no change in control samples (Figure 2.11). This suggests that increased detection of PCSK9 in the experimental group prior to IgG removal was largely due to the presence of Ig-bound rather than free PCSK9.

Discussion

PCSK9 has become one of the most promising therapeutic targets in cardiovascular research since the observation in 2003 of its role in a form of autosomal dominant hypercholesterolemia [41]. Subsequent elucidation of the biology of the protein and observations of the metabolic consequences of gain-of-function and loss-of-function mutations have suggested that simply blocking its ability to bind LDL-R would be sufficient to neutralize its activity and significantly lower potentially pathological circulating LDL-C [48, 60, 61]. These features make PCSK9 an ideal candidate for monoclonal antibody therapy. However, monoclonal antibodies are expensive to manufacture and are also relatively short acting. In this study, we have shown that active immunotherapy, when used to generate a neutralizing antibody response targeting PCSK9, may be an effective alternative to monoclonal antibody

therapeutics. We generated a panel of VLP-based vaccines, utilizing multiple bacteriophage platforms for display of an array of human-PCSK9 derived peptides that were chosen for their surface exposure and proximity to the LDL-R binding site. We then assessed their ability to generate high titer IgG responses as well as to lower circulating lipids in immunized mice. We were able to generate medium- to high-titer peptide-specific and recombinant human PCSK9-reactive IgG responses with each bacteriophage VLP platform tested (Figures 2.4-6), and several vaccine candidates were identified that significantly lowered circulating lipid levels, most notably Qβ-PCSK9$_{207\text{-}223}$.

Immunization with Qβ-PCSK9$_{207\text{-}223}$ caused most dramatic decreases in all lipid parameters investigated in Balb/C mice (Figure 2.8), and caused a significant decrease in triglycerides in a study using C57BL/6 mice fed a high-fat Western diet as well as durable peptide titers out to 6 months (Figure 2.9). A reduction in triglycerides in both mouse strains was particularly encouraging. While humans carry the majority of circulating cholesterol on potentially pathological LDL particles, mice carry ~70% of total circulating cholesterol on high-density lipoprotein (HDL) particles, and are particularly resistant to cardiovascular disease because this type of lipid particle does not deposit cholesterol in blood vessel walls in contrast to LDL and VLDL particles [62, 63]. In mice therefore, total cholesterol is not as predictive of cardiovascular disease as in humans, and to test the effects of a PCSK9-targeted therapeutic that increases cell-surface LDL-R, there are several more relevant plasma lipid metrics. Triglycerides are the main component of chylomicrons and VLDL (the latter of which are converted to LDL by loss of some of

their triglycerides to tissues that require this form of energy), and the remnants of these circulating lipoproteins are eventually cleared from circulation via liver LDL-R. As circulating triglyceride levels are dependent on the presence of liver LDL-R, the target of PCSK9, they represent valuable plasma markers for comparing PCSK9-tageted therapeutics. In addition, the bulk of free cholesterol and phospholipids are transported on LDL particles in plasma, so those were two other metrics used in this study. Each of these parameters decreased significantly in groups of Balb/C mice immunized with Qβ-PCSK9$_{207\text{-}223}$.

In addition to being located near the LDL-R binding site, characteristics of this PCSK9 epitope include a structurally disordered loop, spanning amino acids 213-218, as well as a cleavage site for proprotein convertase furin between residues 218 and 219 [44, 45]. Furin-cleaved PCSK9 is unable to degrade LDL-R, and several naturally occurring gain-of-function mutations in this region may therefore decrease cleavage and hence decrease inactivation of PCSK9 [39, 40]. While these studies would suggest that targeting of this region might prevent physiologic turnover of PCSK9, our data indicate that antibody binding to PCSK9 at this site may neutralize PCSK9 despite prevention of furin cleavage. This region of PCSK9 is highly conserved among almost all vertebrates [64]. It was reasonable therefore to expect that we could elicit a mouse-PCSK9 cross-reactive IgG response with this vaccine, and indeed we were able to show this indirectly by depleting plasma of vaccine-elicited IgG-bound mouse PCSK9 in the Qβ-PCSK9$_{207\text{-}223}$-immunized sera but not control sera (Figure 2.11).

High sequence conservation in the 207-223 epitope contrasts the 68-76 epitope targeted by a different Qβ-based vaccine examined in this study; the human and mouse sequences of targeted epitopes are listed in Table 2.1. The human 68-76 sequence that we used in this vaccine has only ~65% sequence homology with mouse PCSK9. Thus, the sequence heterogeneity of this region may explain the relative lack of functionality of antibodies generated by the vaccine, since similar titers of anti-peptide and anti-human PCSK9 antibodies were elicited in this as compared to the other Qβ-based vaccines (Figure 2.6). The additional peptides tested exhibit almost complete homology between human and mouse PCSK9 amino acid sequence, and may have had varied lipid outcomes for reasons other than poorly cross-reactive antibody responses. For example, the location of the epitope targeted on PCSK9 in relation to the LDL-R binding site likely affected neutralization capacity of vaccine-elicited IgG. In the case of most of the peptides tested, it seems reasonable that an antibody molecule bound to the epitope would directly block or sterically inhibit the interaction of PCSK9 and LDL-R (Figure 2.1). In the case of the PCSK9 (68-76) and (153-163) peptides though, it is possible that PCSK9 bound by an IgG molecule at one of these sites might still be functional and able to bind LDL-R and promote its degradation. Alternatively, the targeted sites may be less readily accessible to antibody as compared to the (207-223) surface-exposed loop.

In addition to testing a variety of PCSK9 epitopes, we also compared different methods of VLP-based display. Different valency and level of constraint of peptide presentation are achieved when the same epitope is displayed by either conjugation to Qβ, or genetic insertion within the AB-loop of PP7 coat protein or at the N-

terminus of MS2 coat protein (Figure 2.2). A comparison of Qβ and MS2 VLPs displaying the 153-163 epitope revealed that Qβ display elicited 10-100 fold higher anti-peptide and anti-PCSK9 IgG titers than MS2 display (Figures 2.5). This may be explained by the density of peptides displayed on each VLP, which is higher for Qβ (typically 1-3 peptides per coat protein, or 180+ peptides per VLP) as compared to either MS2 or PP7 (1 peptide per coat protein dimer, or 90 peptides per VLP). VLP vaccine type-dependent decreases in lipid levels were compared by relative triglyceride and total cholesterol levels before and after immunization (Figure 2.7A and B), and while no significant difference in relative triglyceride levels were found between groups, the decrease in total cholesterol relative to preimmune levels was found to be significantly greater in the Qβ group compared to the MS2 group (mean change of 0.66±0.18 for Qβ and 0.90±0.11 for MS2). This is likely related to the higher titer IgG responses elicited by the Qβ-based vaccine that promotes increased neutralization of PCSK9, and which is in turn a function of valency [12, 57].

In summary, we have investigated a panel of potential PCSK9-targeting vaccines, and identified at least one candidate for future study. It will be important to show that this vaccine is effective at decreasing LDL-C in non-human primates (whose lipid metabolism closely resembles that of humans), and that the lipid-lowering effects are durable. Exciting work has been shown recently translating PCSK9-targeting monoclonal antibody therapies into primates as well as humans in late stage clinical trials, with very limited side effect profiles [50, 65], and we anticipate similar results with our vaccine given the promising preliminary data presented

here. VLP-displayed PCSK9 peptide would be an extremely cost-effective alternative to other therapies that will likely be as widely used as statins, potentially complementing that form of therapy. Considering the increasing rate of cardiovascular disease worldwide, these therapies will play an important role in human health.

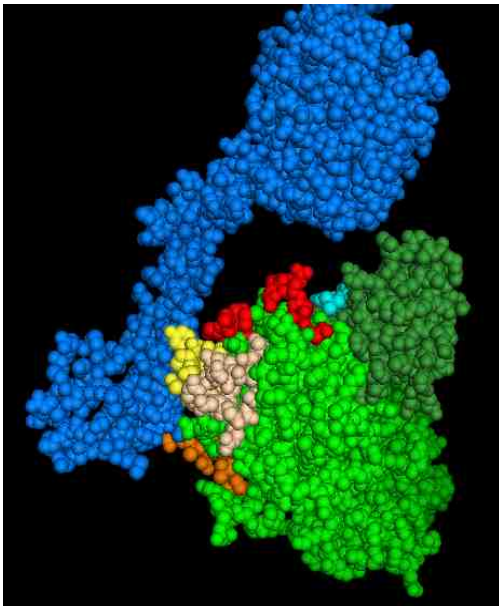

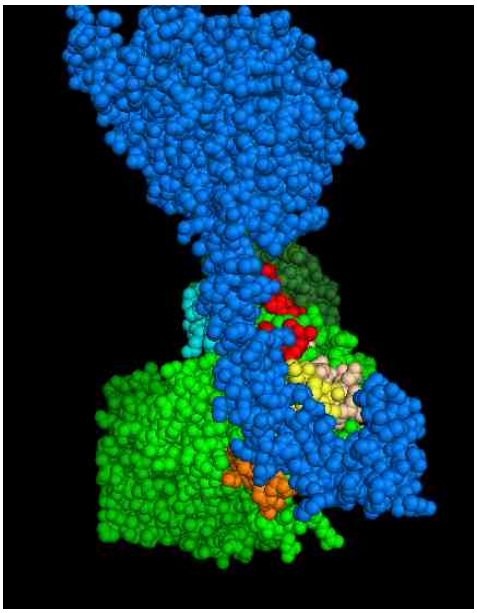

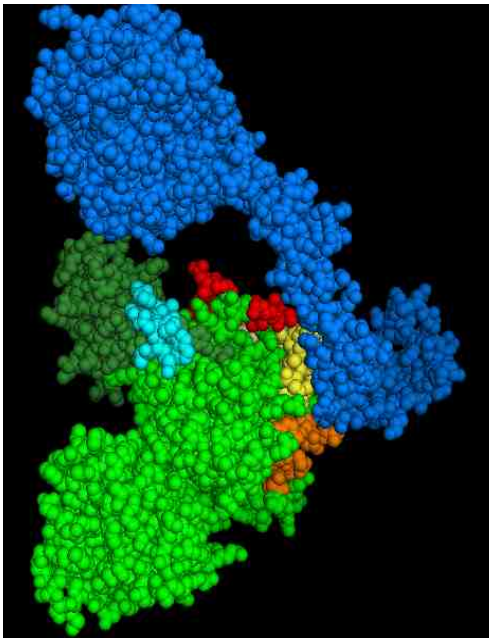

Figure 2.1. The crystal structure of PCSK9 in complex with the extracellular domain of LDL-R, and strategies used to target the binding site. The prodomain and catalytic domain of human PCSK9 are shown in dark and light green, respectively; the extracellular domain of LDL-R is shown in dark blue. The PCSK9-derived peptides investigated in this study are also shown, and are described by color and sequence in the chart below. Also included in the chart are descriptions of the method(s) of display used for each peptide. These images were generated using the coordinates provided by the RCSB protein data bank using the program PyMOL.

PCSK9 peptide	Amino acid sequence (human PCSK9)	Method of display: Chemical conjugation	MS2 N-terminus	PP7 AB-loop
hPCSK9 (207-223)	NVPEEDGTRFHRQASKC	√	√	
hPCSK9 (153-163)	SIPWNLERITP	√	√	
hPCSK9 (68-76)	AKDPWRLPG	√		
hPCSK9 (368-381)	IIGASSDCSTCFVS		√	√
hPCSK9 (188-200)	SIQSDHREIEGRV		√	√

A 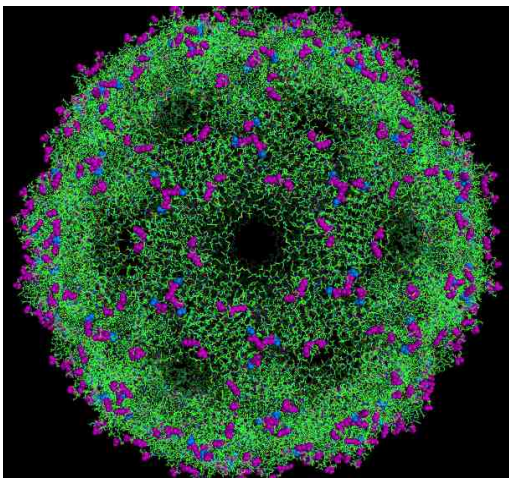 B 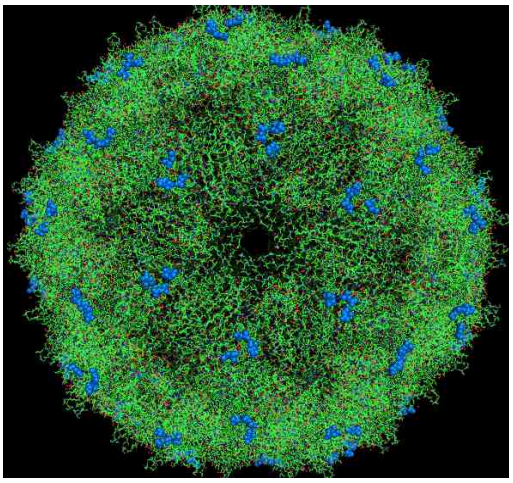

C 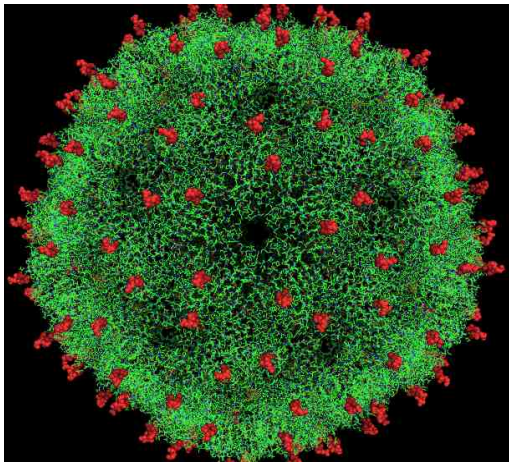

Figure 2.2. Crystal structures of the bacteriophage capsids used as VLPs. Panel A shows the Qβ bacteriophage capsid, with surface-exposed lysines depicted in purple and N termini depicted in blue; panel B shows the MS2 capsid, with N termini depicted in blue; panel C shows the PP7 capsid, with surface-exposed AB loops shown in red. These images were generated using the coordinates provided by the VIPER database using the program PyMOL.

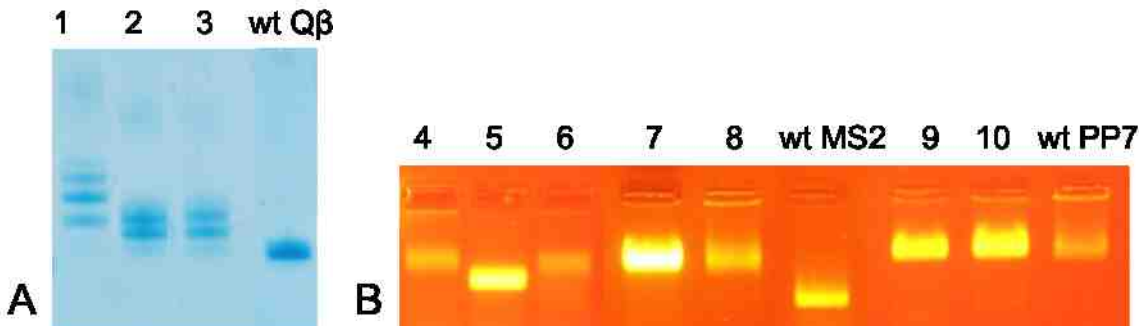

Figure 2.3. Generation of VLPs displaying PCSK9 peptides. Panel A shows an SDS-PAGE of conjugated Qβ VLPs, using hPCSK9 peptides 207-223 (1), 153-163 (2) or 68-76 (3). Panel B shows an agarose gel of recombinant MS2 (4-8) and PP7 (9-10) VLPs, using hPCSK9 peptides 213-222 (4), 153-163 (5), 208-222 (6), 188-200 (7, 9) and 368-381 (8, 10).

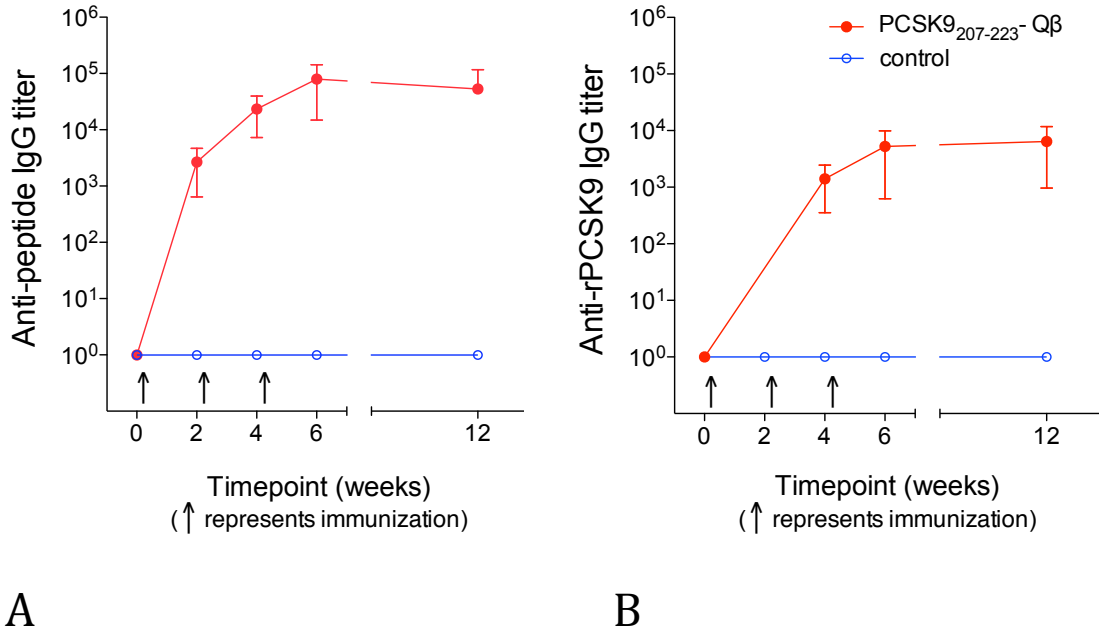

Figure 2.4. Peptide- and recombinant hPCSK9-reactive IgG titers elicited by immunization. PCSK9 peptide (207-223) conjugated to Qβ is shown as a representative, but all Qβ-based vaccines elicited $10^{4\text{-}5}$ peptide-specific IgG responses (A). IgG reactive to recombinant human PCSK9 is also shown for the representative vaccine, but each vaccine elicited PCSK9-reactive titers over 10^3 (B). Mean and standard deviation (SD) are shown.

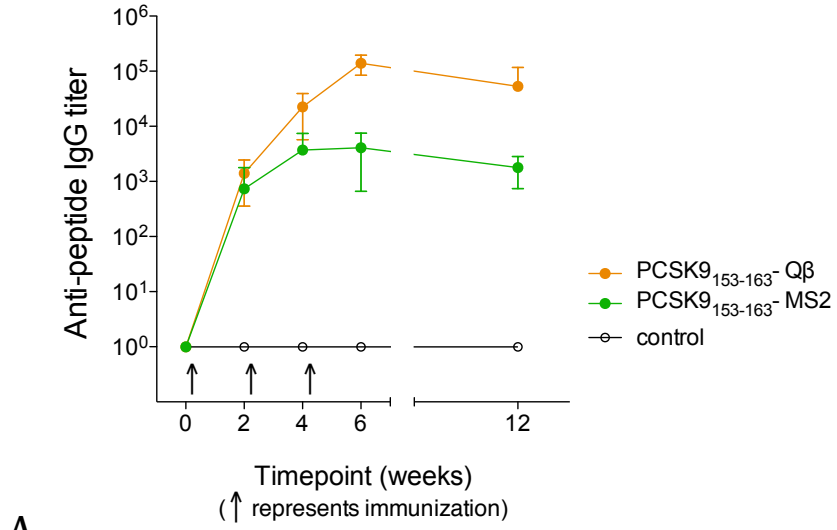

A

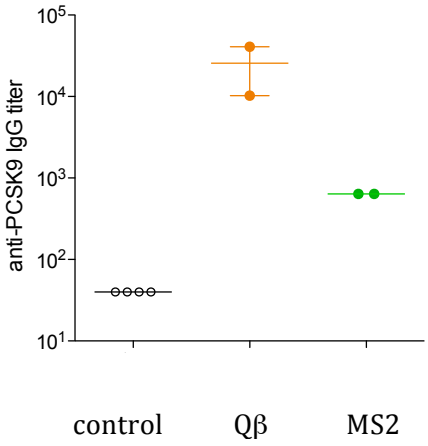

B

Figure 2.5. Qβ elicits higher titers than MS2 when used to display identical peptide. PCSK9 peptide (153-163) conjugated to Qβ is shown in red filled circles, and MS2 N-terminal display of the peptide is shown in green filled circles. Empty circles represent wild-type VLP-immunized controls. Mean and SD are shown for anti-peptide titers (A), and mean reactivity of pooled plasma samples is shown for anti-PCSK9 titers (B).

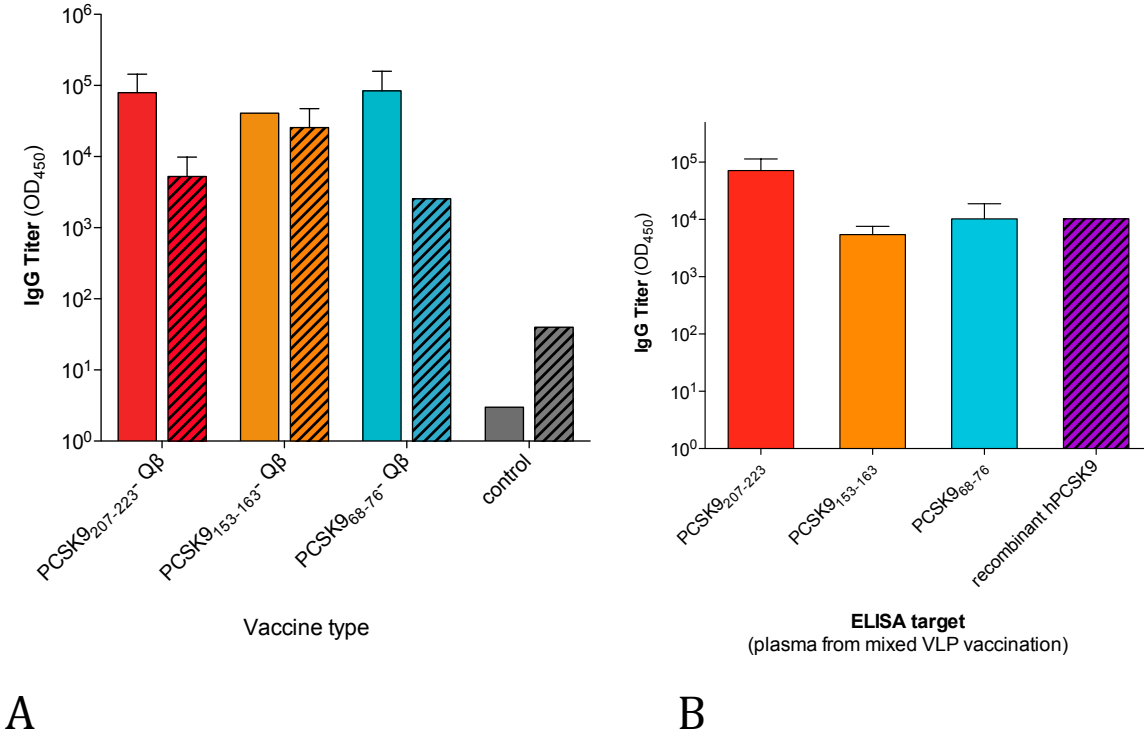

Figure 2.6. Peptide- and recombinant hPCSK9-reactive IgG titers elicited after immunization with Qβ-based vaccines. PCSK9 peptide-specific responses are shown in solid bars, and reactivity with recombinant hPCSK9 is shown in hatched bars. Panel A compares separate vaccines given individually, while panel B shows the individual peptide and PCSK9 responses elicited by a vaccine consisting of a mix of the three VLPs. Mean and standard error of the mean (SEM) are shown for reactivity of pooled plasma samples.

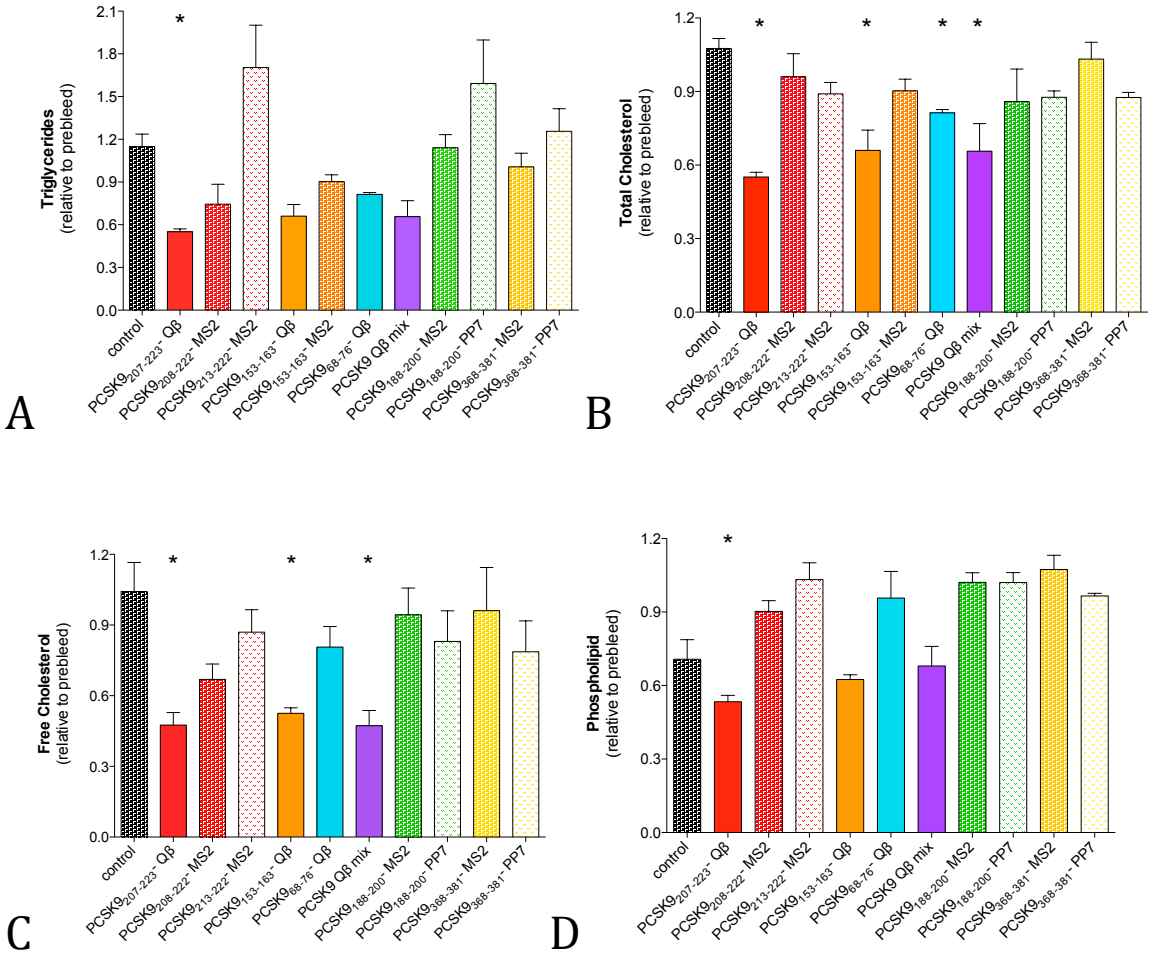

Figure 2.7. Relative circulating lipid levels in immunized mice. Triglycerides (A), total cholesterol (B), free cholesterol (C) and phospholipids (D) were measured in preimmune plasma samples and after three immunizations, and relative values obtained for each individual sample. Mean and SEM are shown; * denotes a significant decrease ($p < 0.05$) in lipid level of experimental group compared to control by independent 2-tailed t-test, using Levene's test to account for unequal variance when necessary. In panels A and B, control group includes both 5 wt Qβ- and 5 wt MS2-immunized mice. Panels C and D control group includes 5 wt Qβ-immunized mice only.

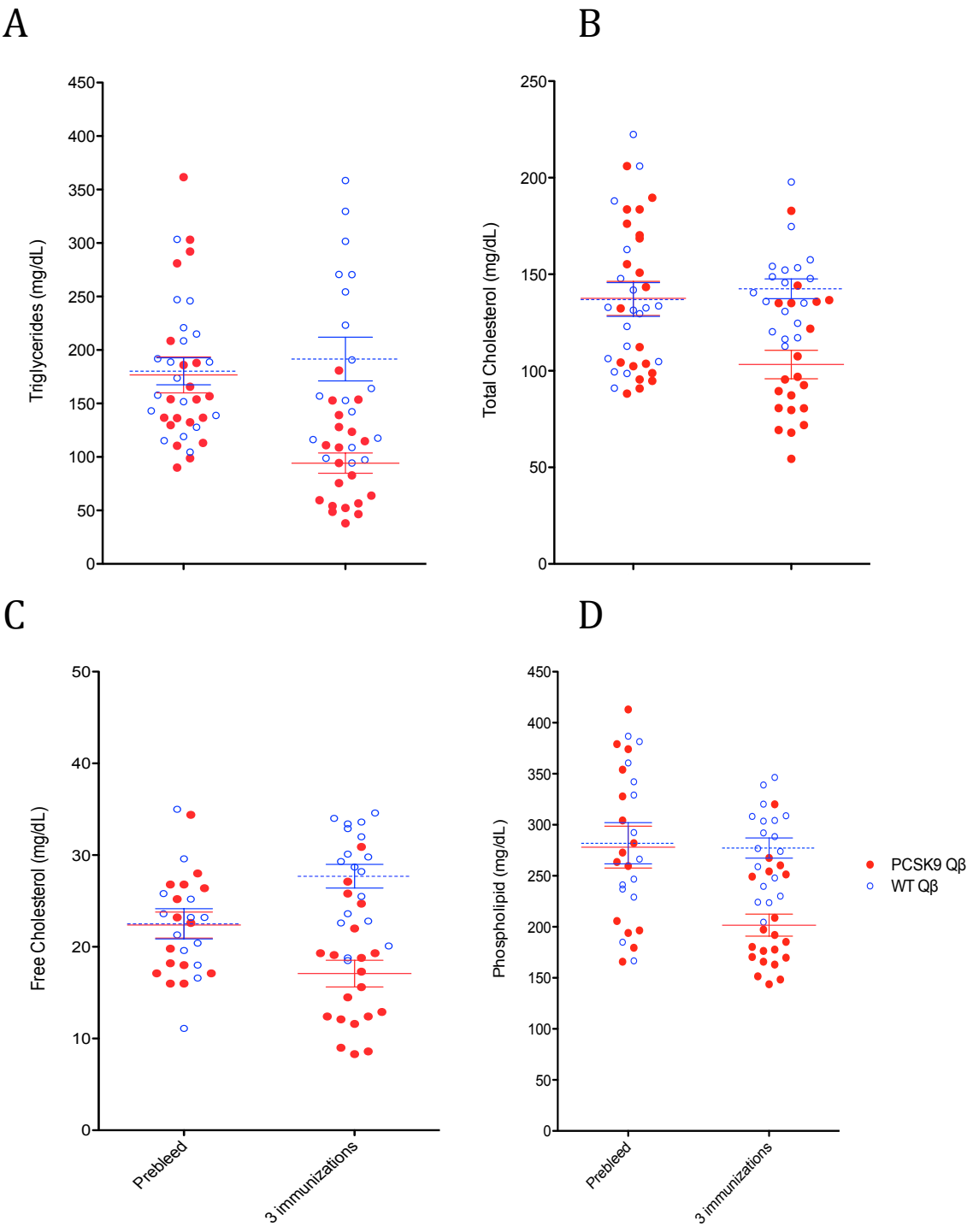

Figure 2.8. Quantification of plasma lipids in mice, before and after immunization with $PCSK9_{207\text{-}223}$Qβ. Red/filled circles show Qβ-PCSK9 (207-223)-immunized mouse plasma samples, and blue/empty circles show control-immunized samples. Mean and SEM are shown for triglycerides (A), total cholesterol (B), free cholesterol (C) and phospholipids (D); significant differences were seen in each lipid parameter at the final time point ($p < 0.001$), while no initial significant differences were seen.

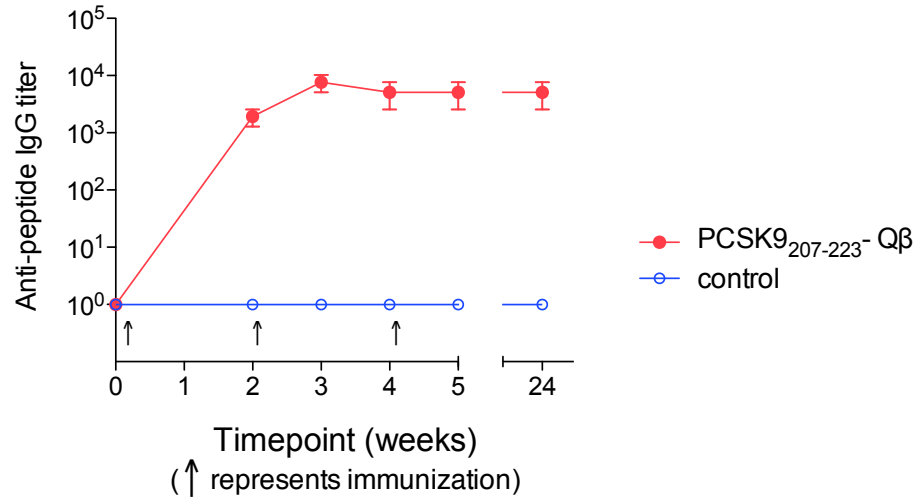

A

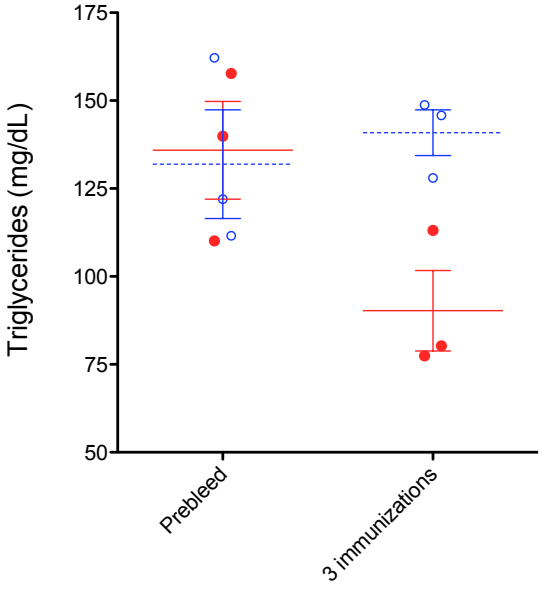

B

Figure 2.9. Quantification of peptide titers and plasma triglycerides in immunized C57BL/6 mice fed a Western diet. Red/filled circles show Qβ-PCSK9 (207-223)-immunized mouse plasma samples, and blue/empty circles show control. Mean and SEM are shown for peptide titers elicited over the course of 3 immunizations (A), and for plasma triglyceride levels before and after all immunizations (B). A significant difference was seen at the final time point in triglyceride levels ($p < 0.05$), while no initial significant difference was seen.

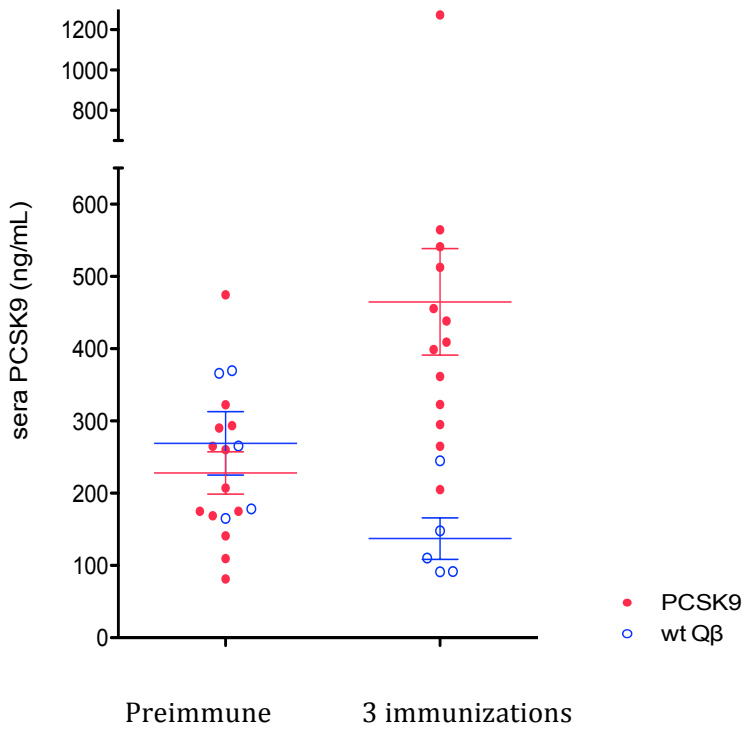

Figure 2.10. Quantification of plasma PCSK9 in mice, before and after immunization. Red/filled circles show Qβ-PCSK9 (207-223)-immunized mouse plasma samples, and blue/empty circles show control-immunized samples. Mean and SEM are shown; significant difference between experimental and control groups observed at final time point only ($p < 0.05$).

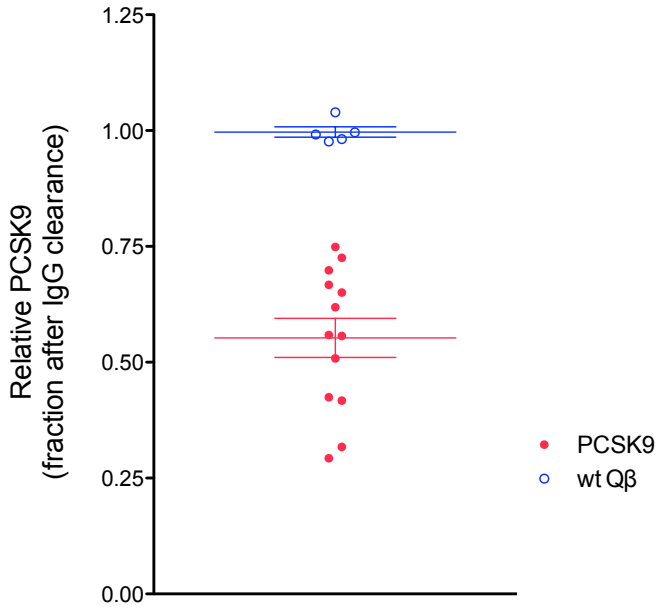

Figure 2.11. Effect of depleting plasma of IgG on PCSK9 detection. Red/filled circles show relative PCSK9 depletion from Qβ-PCSK9 (207-223)-immunized mouse plasma samples, and blue/empty circles show no depletion from control-immunized samples. Mean and SEM are shown; significant difference between experimental and control groups observed ($p < 0.05$).

Table 2.1

PCSK9 (human) peptide	Amino acid sequence of human PCSK9 (mouse PCSK9)	Method(s) of display	Forward primers for genetic insertion
hPCSK9 (207-223)	N-VPEEDGTRFHRQASKC (NSVPEEDGTRFHRQASKC)	MS2 N-terminal genetic insertion (MS2-N) Qβ conjugation	ATGCGCCATGGCAGTG CCGGAAGAAGATGGC ACCAGATTTCATAGAC AGGCGTCTAAAGGCGG CGGCAGCTCAACCGGA GTTGGAAGC
hPCSK9 (213-222)	GTRFHRQASK (conserved)	MS2-N	ATGCGCCATGGCAGGC ACCAGATTTCATAGAC AGGCGTCTAAAGGCGG CGGCAGCTCAACCGGA GTTGGAAGC
hPCSK9 (188-200)	SIQSDHREIEGRV (SIQGAHREIEGRV)	MS2-N PP7 AB-loop genetic insertion (PP7-AB)	ATGCGCCATGGCAAGC ATTCAGAGCGATCATC GTGAAATTGAAGGCC GTGTGGGCGGCGGCAG CTCAACCGGAGTTGGA AGC; GGCTCGGTACCAGCAT TCAGAGCGATCATCGT GAAATTGAAGGCCGT GTGGAGGCTACTCGCA CTCTGACTGAG
hPCSK9 (368-381)	IIGASSDCSTCFVS (IIGASSDCSTCFMS)	MS2-N PP7-AB	ATGCGCCATGGCAATT ATTGGCGCGAGCAGCG ATTGCAGCACCTGCTT TGTGAGCGGCGGCGGC AGCTCAACCGGAGTTG GAAGC GGCTCGGTACCATTAT TGGCGCGAGCAGCGAT TGCAGCACCTGCTTTG TGAGCGAGGCTACTCG CACTCTGACTGA
hPCSK9 (153-163)	SIPWNLERITP (SIPWNLERIIP)	MS2-N Qβ conjugation	ATGCGCCATGGCATCT ATTCCGTGGAATCTGG AAAGAATTACCCCGGG CGGCGGCAGCTCAACC GGAGTTGGAAGC
hPCSK9 (68-76)	AKDPWRLPG (SKEAWRLPG)	Qβ conjugation	

Chapter 3: Affinity selection with the malaria-neutralizing antibody 4G2 using a bacteriophage virus-like particle platform for vaccine discovery

Abstract

Identifying and targeting complex neutralizing epitopes on pathogens is a major hurdle in vaccine development, despite recent advances in epitope mapping and molecular design techniques. One strategy has been to screen peptide libraries displayed on filamentous bacteriophages by affinity selection, using monoclonal antibodies with known (and desirable) function. This approach has provided efficient means for epitope identification as well as discovery of mimotopes, or short peptides that mimic complex epitopes and by definition should elicit a neutralizing response against the native epitope. However, filamentous phages are poorly immunogenic because they fail to present foreign epitopes at the high densities required for efficient B-cell activation. They therefore make poor vaccine platforms for identified mimotopes, which have largely failed to translate as vaccines when displayed on other more immunogenic platforms. Meanwhile, systems based on virus-like particles permit the engineered high-density display of short peptide epitopes. We have previously developed a peptide display platform based on VLPs of the RNA bacteriophage MS2 that combines the high immunogenicity of VLP display with affinity selection capabilities. Specific or random peptides can be displayed on the VLP surface by genetically inserting a sequence into a surface-exposed loop of the viral coat protein. VLP-displayed peptides can then be isolated

by specific antibody screening, and the VLP selectants used directly as immunogens. We have previously shown that >95% of insertions are compatible with VLP assembly, using random peptide sequences of either 6, 7, 8 or 10 amino acids. Here we have investigated the ability of this platform to identify mimotopes of a conformational epitope present on the highly conserved malaria protein AMA1. Using 4G2, a monoclonal antibody that binds to a conserved region of AMA1 and is a potent inhibitor of erythrocyte invasion, we screened VLP-displayed random peptide libraries and identified several peptides that may be acting as mimotopes of the 4G2 epitope in the context of the VLP platform. One of the selected VLPs elicited antibodies that bound to AMA1, and may be a potential vaccine candidate.

Introduction

Virus-like particles (VLPs) derived from the coat proteins of many different viruses have been used as vaccines. VLPs can be used to target the virus from which the VLP is derived, or alternatively can be used as platforms to greatly increase the immunogenicity of heterologous antigen presented on the VLP surface [4, 66, 67]. Linking target antigens, either genetically or chemically, to the surfaces of VLPs causes them to be displayed at high density. This high-density display, in turn, dramatically enhances the ability of linked antigens to induce antibody responses [8, 24]. Although many target-specific VLP-based vaccines have been engineered [68], in the past VLP technology has not been adapted for use in epitope identification. Largely this is because recombinant VLPs are not well suited for the construction of diverse peptide libraries. However, we have developed a strategy whereby we can

generate large, diverse libraries of VLPs displaying random peptides, and then discover vaccines from this library by using affinity selection [3, 39].

The use of the MS2 VLP for affinity selection applications (shown schematically in Figures 3.1 and 3.2) depends on three key features: 1) a surface-exposed site in coat protein that tolerates insertions without disruption of coat protein folding or VLP assembly, 2) the encapsidation of nucleic acid that encodes the coat protein and any guest peptide it displays, allowing recovery of the genetic material post-selection, and 3) the ability to increase the stringency of selection by reducing target valency. To satisfy the first requirement, we have engineered the viral structural coat protein of MS2 to allow display of random peptide libraries in a high-density array on the surface of formed recombinant VLPs. MS2 VLPs are formed by self-assembly of 90 homodimerized coat proteins, resulting in a T=3 icosahedral particle (Figure 3.3). In our system, peptides are genetically inserted into a surface-exposed loop on the phage coat protein. We have shown that peptide insertions at this site are almost universally (>95%) tolerated when the downstream copy of two coat proteins in a genetically fused 'single-chain dimer' is used [3, 4, 32]. Thus we can display random peptides on MS2 VLPs, facilitating the construction of diverse peptide libraries. The second requirement is satisfied by the ability of recombinant VLPs to encapsidate the mRNA that encodes coat protein and any guest peptide it carries. This enables amplification of recovered peptide selectant sequences from VLPs over multiple rounds of affinity selection by RT-PCR. The third requirement has been addressed using two methods. First, we may increase competition among VLPs by limiting the amount of selecting antibody available. Second, we have engineered a single-chain

dimer with a repressible stop codon between the two copies of coat protein, only the downstream copy of which contains the peptide insert. By transforming a bacterial strain that contains a repressor tRNA with known efficiency, we allow a predictable frequency of read-through. In this way VLPs with a quantity of insert-containing single-chain dimer as well as wild type dimers (and therefore with fewer peptides displayed on the surface) can be generated. This decreases the probability that VLPs will be selected by avidity interactions and rather as high-affinity mAb binders.

Using these methods, we can affinity select recombinant VLPs from highly diverse (10^{10}) random libraries using mAbs of interest. The ability to identify epitopes on the same structural platform to be used later in their presentation as a vaccine increases the likelihood that selected VLPs will be able to elicit antibodies with activities mimicking those of the selecting antibody [69]. We believe this process can be applied for direct identification of highly immunogenic vaccine candidates displaying mimotopes of complex epitope targets. As a proof of principle, we have previously screened mAbs that recognized defined linear epitopes with our MS2 VLP library. We were able to select VLPs displaying peptides with remarkable homology to these epitopes, and the selected recombinant VLPs induced high-titer antibody responses with similar activity to the selecting mAb [39]. In this way, by providing a platform for vaccine discovery in the context of the intended immunogen, we have developed a powerful tool for use in affinity selection, and have extended the concept here to identifying mimotopes of a malaria parasite-neutralizing mAb that recognizes a conserved conformational epitope.

Malaria has been one of the most difficult parasitic pathogens to target with vaccines. The *Plasmodium* parasite encodes more than 5,000 proteins in its genome, many of which are highly variable between strains, and undergoes 3 separate life stages in humans and mosquitoes (the vectors for transmission). The parasite is able to infect both hepatocytes and erythrocytes in humans, using different mechanisms for attachment and entry in each case [70, 71]. The clinical manifestations of malaria occur during the blood-stage life cycle of the parasite, after rupture of hepatocytes releases merozoite forms into circulation. Merozoites invade erythrocytes, and mature into trophozoite then schizont parasitic forms, eventually rupturing cells and releasing daughter merozoites [72]. These merozoites can initiate a new cycle of replication in erythrocytes. Several blood-stage protein targets have been studied and prioritized as vaccine targets, and one of the foremost is apical membrane antigen-1 (AMA1) [73]. Critical functions of this merozoite surface protein in erythrocyte invasion have been described recently, and have shed light on conserved epitopes that may be targeted by vaccines [21, 74]. While the protein has highly polymorphic and strain-specific regions, it also contains conserved regions that are critical in erythrocyte invasion [19, 75], and antibodies that bind this type of region hold the most promise for affinity selection-based vaccine development.

Naturally acquired immunity to malaria requires long-term and continuous exposure [76], but immunization studies in animals with recombinant protein as well as screening of infected human sera have revealed that AMA1-specific mAbs capable of neutralizing diverse strains of *Plasmodium* parasites can be elicited [77-

79]. In contrast, immunization with reduced AMA1 protein failed to elicit parasite-neutralizing Abs, suggesting that conformational epitopes are responsible for the neutralization seen in recombinant AMA1 immunization [78]. Early human trials with recombinant AMA1 derived from various strains have shown high anti-AMA1 titers may be elicited [80, 81], but immunodominant epitopes on AMA1 are largely strain-specific and fail to provide protection after multiple malaria seasons [82-84]. While new vaccines containing recombinant protein derived from several *Plasmodium* strains are currently being pursued in animal studies [85], these may also fail to provide neutralizing universal coverage in humans over time. Alternatively, by specifically targeting conserved regions of critical function on AMA1 with an epitope-based vaccine, issues of antigenic variation may be avoided. To this end, we have chosen the parasite-neutralizing mAb 4G2 as a candidate to use in our affinity selection strategy.

4G2 is one of the most broadly inhibitory anti-AMA1 antibodies yet identified, and recognizes a conserved face of the protein (Figure 3.4) [86-88]. Passive transfer studies with this mAb have shown protection in animal models [89], and it recognizes a conformational epitope as it fails to bind denatured AMA1 protein [90]. The mechanism of action of 4G2 in preventing erythrocyte invasion appears to be blocking of AMA1 binding to another merozoite protein RON2 [19], and the site of 4G2 binding is indeed in close proximity to a hydrophobic trough critical in this interaction [91]. Filamentous phage display and affinity selection using this mAb have been performed previously [92], however the peptides thus identified have not translated as vaccine candidates. For these reasons, and because the 4G2 epitope

has been somewhat resistant to rational vaccine design [93, 94], we consider 4G2 an ideal candidate to extend our VLP affinity selection strategy to mimotope identification, with the potential for vaccine development.

Materials and Methods

Construction of plasmid libraries. The plasmids used to construct recombinant VLPs have been described previously [3, 39]. Briefly, plasmids encoding two copies of MS2 coat protein in a single-chain dimer format were used. The upstream copy was 'codon-juggled' to allow discrimination of annealing sites by primers during RT- and PCR steps. The plasmids contained the phage T7 promoter and terminator regions from the pET3d vector, the kanamycin resistance gene and an M13 origin of replication. Unique SalI and BamHI restriction sites were engineered upstream and downstream of the insert-containing copy of coat protein, for use in cloning during affinity selection, and a unique KpnI site was present at the site of peptide insertion. A low-valency version of the plasmid contained an amber stop codon between coat protein copies, and was used in conjunction with a plasmid encoding an alanine-inserting/amber-suppressing tRNA. This allowed a predictable frequency of read-through and translation of the insert-containing downstream copy of coat protein.

The coat protein-encoding plasmids were used in conjunction with the helper phage M13CM1 (a derivative of M13K07 with chloramphenicol resistance rather than kanamycin) to generate ssDNA plasmid, which is isolated from phagemids and used as template for site-directed mutagenesis. Mutagenic primers were targeted to the downstream copy of coat protein overwriting the KpnI site, and contained inserts of

$(NNS)_x$ where x represents 6, 7, 8 or 10 repeats. This format allows the incorporation of any of the 20 amino acids within the random peptide insert, while precluding two of three possible stop codons. KpnI restriction was used to eliminate wild type plasmid, and insert-containing plasmid libraries were used to transform bacterial strain 10G cells (Lucigen). The resulting amplified libraries contained 10^{8+} individual recombinant plasmids.

Production of recombinant VLP libraries. Individual plasmid libraries were used to transform C41(DE3) cells for production of recombinant VLP libraries. We were careful to maintain the diversity represented in the plasmid library by accepting only high efficiency of transformation (10^{8+}) at this step. VLPs were isolated from 100-500mL bacterial cultures grown in LB to OD 0.6 then induced for 3-5 hours with IPTG. Purification was performed by lysis of freeze-thawed cell pellets using a lysozyme solution, followed by addition of deoxycholate, then sonication and DNase treatment as previously described [4]. After centrifugation to remove cellular debris, VLPs were purified on a sepharose CL4B chromatographic column, and VLP-containing fractions were identified by agarose gel electrophoresis and pooled.

Production of mutagenic library based on 10-mer selectant. To generate a VLP library based on a selected 10-mer VLP clone, we constructed a mutagenic plasmid library by randomizing the selectant insert nucleotide sequence. Site-directed mutagenesis was performed using ssDNA from the amber-containing low-valency plasmid as described above. Mutagenic primers were designed through Integrated DNA Technologies as follows. Each of the 30 nucleotide positions encoding the

randomized insert in the primer was incorporated with a mix of nucleotides, weighted 76% to the original sequence nucleotide and 8% each other nucleotide (verified in Table 3.1). This library was otherwise expressed and purified as described above.

Affinity selections. All affinity selections were performed with the mAb 4G2, which was a gift from Dr. David Narum (Laboratory of Malaria Immunology and Vaccinology, NIAID/NIH). Briefly, 4G2 was diluted in PBS and adsorbed onto 96-well Immulon 2 plates (ThermoScientific) overnight at 4°C. In the first 1-3 round(s) of selection, 250ng/well of selecting Ab was used; in the final round of each selection 50ng/well of 4G2 was used (a chart describing number of rounds and VLP valency at each round in individual selections is included in Figure 3.2). Wells were washed (between each step) 5 times with PBS. Wells were then blocked for 2 hours at room temperature with 0.5% dry nonfat milk diluted in PBS. VLP libraries were added at 5-10ug/well in the first round (with equal volumes of 6-, 7-, 8- and 10-mer libraries in the case of the mixed library selection), which was diluted in blocking solution for a total volume of 50uL. In later rounds, 10-25uL/well of 'crude lysate' VLPs were used, purified as above but without sepharose column chromatography and with an additional freeze/thaw step followed by centrifugation. Bound VLPs were eluted by applying 50uL of 0.1M glycine, pH 2.7 for 8 minutes, followed by neutralization with 5uL 1M Tris, pH 9.0.

Reverse transcription was performed using 5-10uL of eluate with 2pmol of a primer annealing downstream of the single-chain dimer and MLV reverse transcriptase

(Invitrogen) as per manufacturers' instructions. The DNA product was amplified by PCR using Taq DNA polymerase (Invitrogen) as per manufacturers' instructions with primers annealing up- and downstream of the insert-containing copy of coat protein, and preserving the unique restriction sites described above. The amplified product was digested using BamHI and SalI restriction enzymes, and the resulting product was cloned into either the high- or low-valency plasmid expression vector for additional rounds of affinity selection.

Relative binding of individual selectant VLPs and libraries. Relative binding was determined by capture ELISA, comparing binding of VLP libraries or individual selectant VLPs to 4G2 *vs.* an isotype control mAb (rat IgG2; Jackson ImmunoResearch). Individual selectants were isolated by transforming C41(DE3) cells with 1-10pg of plasmid (to ensure 1 plasmid per bacterial colony), letting the bacteria recover for 1 hour in a small volume of SOC, then plating on kanamycin agar plates. Single colonies were lysed by freeze/thaw of the pellet, then resuspended in sepharose column buffer and sonicated. DNase treatment and a final centrifugation step were performed, and the soluble VLPs were recovered in the supernatant.

Either 4G2 or isotype mAb was adsorbed onto 96-well Immulon 2 plates (ThermoScientific) at 250ng/well overnight at 4°C. Duplicate wells were washed (between each step) 5 times with PBS. Wells were then blocked for 2 hours at room temperature with 0.5% dry nonfat milk diluted in PBS. VLP libraries from each round of selection, or individual VLP selectants, were diluted in blocking solution

and added to both 4G2- and isotype-coated wells at equal concentrations (as determined by denaturing gel electrophoresis) and at several dilutions, for 2 hours at room temperature. Captured VLPs were incubated with rabbit anti-MS2 polyclonal sera for 1 hour at a 1:2,000 dilution in blocking solution, and detected by peroxidase-conjugated goat anti-rabbit IgG antibody (Jackson ImmunoResearch; 1 hour, 1:5,000 dilution). ABTS substrate was used and the reaction was read at OD_{405}. OD values of 4G2 mAb wells were normalized to isotype control mAb wells and the ratio was reported.

Deep sequencing of plasmid libraries and sequencing of individual selectant VLP plasmids. Individual selectant VLP plasmids were purified by picking individual colonies as above and allowing overnight small-volume growths. Qiagen QIAprep miniprep kits were used as per manufacturers' instructions to purify plasmid, which was sent to Eurofins MWG Operon for sequencing of individual selectants. Deep sequencing was performed on intermediate and final round mutagenic and mixed VLP libraries as follows. KpnI-restricted plasmid libraries were used as template in PCR reactions, performed using a bar-coded forward primer and universal reverse primer for each sample. Total PCR product was isolated by agarose gel purification using a Qiagen QIAquick gel extraction kit. Each bar-coded sample was then mixed at equal concentrations and Dr. Jeremy Edward's lab performed Ion Torrent sequencing (Life Technologies). Raw nucleotide sequence data was extracted and translated to peptide insert sequences by Dr. Kathryn Frietz. Peptide selectants were ranked according to number of reads of each unique sequence, and percent representation for each selectant was calculated by dividing the number of

individual peptide reads by total reads in the same bar-coded sample. Fold-enrichment for each selectant was calculated by dividing the percent representation of each peptide in the final round by its percent representation in the preceding round.

Assessment of affinity-selected peptide families. The final round selectants in the mixed library selection were sorted into families using the online Immune Epitope Database analysis resource [95]. Limiting our analysis to the top ~1,450 unique peptide selectants, we set the sequence identity threshold to 80% in the Epitope Cluster Analysis tool and extracted families of at least 10 members. Consensus sequences were ascertained for each family using the online WebLogo resource [96].

Immunogenicity of recombinant VLP selectants. Individual VLP selectants were isolated and purified as above, or cloned independently using site-directed mutagenesis (also as above) if no colony was picked with the desired peptide insert. VLP formation was confirmed by agarose gel electrophoresis, and VLPs were purified by sepharose chromatography or FPLC then quantified by denaturing polyacrylamide gel electrophoresis. For the first immunization scheme, using the 10mer VLP selectant, groups of 3-5 Balb/C mice were given two intramuscular immunizations with either 10ug selectant VLP or wild type VLP at 2-week intervals, and sera was drawn by intraocular bleed 2 weeks after the second dose. A recombinant AMA1 boost was also given at this time point (PpAMA1-3D7, a gift from the lab of Dr. David Narum), and consisted of 25ug protein formulated with

50% IFA. Sera was drawn again 2 weeks after AMA1 immunization. A control group received only the AMA1 vaccination. Anti-AMA1 titers were quantified by sera dilution in a direct ELISA, and anti-peptide titers were quantified by engineering a PP7 bacteriophage to display the 10mer sequence in a similar surface-exposed loop to that of MS2. Briefly 500ng/well of recombinant AMA1 or recombinant PP7 VLPs were adsorbed to ELISA plate wells overnight at 4°C. Blocking and washing were performed as above, and dilutions of sera were added to wells. Peroxidase-conjugated goat anti-mouse IgG was used for detection of bound sera IgG (1 hour, room temperature), and either ABTS or TMB (neutralized with 1% HCL) was used as substrate. OD was read at 405nm or 450nm, respectively.

In a second immunization scheme, using the mutagenic and mixed library VLP selectants as well as one group receiving the 10mer VLP selectant used previously, groups of 3 Balb/C mice were given three intramuscular immunizations of 5ug VLP (except 2.5ug for NWDPIQFPGK VLP), formulated with 50% incomplete Freund's adjuvant (IFA; Sigma Aldrich) at 2-week intervals. Sera was taken one week after the final immunization, and anti-AMA1 IgG titers were measured in dilutions of sera by direct ELISA. Sera from wild type VLP immunized animals served as ELISA controls in all experiments.

Immune sera *vs.* 4G2 competition ELISA. A competition ELISA was performed whereby sera from mice immunized with AMA1 only, 10mer selectant VLP only, 10mer VLP-primed/AMA1-boosted or wild type VLP control competed with 4G2 for binding to immobilized AMA1. No sera controls were also included. Briefly,

250ng/well recombinant AMA1 was adsorbed to ELISA plate wells overnight at 4°C. Blocking and washing were performed as above, and dilutions of sera were added to 4G2 (diluted 1:20,000) in triplicate wells. Peroxidase-conjugated mouse anti-rat IgG was used for specific detection of 4G2 (1 hour, room temperature), and ABTS used as substrate. OD was read at 405nm, and all experimental OD values were normalized to the internal no-sera controls for each experiment so that competition could be compared between separate ELISA runs.

Relative affinity of 4G2 for selectants. For the final mutagenic and mixed library VLP selectants, relative affinity was measured by adsorbing 500ng/well of individual VLPs to ELISA plate wells and incubating overnight at 4°C. Blocking and washing were performed as above, and dilutions of 4G2 were added in triplicate wells. Peroxidase-conjugated mouse anti-rat IgG was used for specific detection of 4G2 (1 hour, room temperature; 1:5,000), and TMB used as substrate (neutralized with 1% HCl). OD was read at 450nm.

Results

We used three different approaches in order to identify mimotopes of the 4G2 conformational epitope.

Affinity selection using a 10mer VLP library. In the first affinity selection approach we used our longest peptide-insert VLP library, which displays random 10-amino acid peptides on the surface-exposed AB loop of MS2 VLPs. Four rounds of affinity selection were performed, the first two utilizing high-valency peptide display and the last two utilizing low-valency display. To further increase stringency, we used

less 4G2 (50ng) in the final round of selection. After the final round, we picked 24 individual selectants, sequenced them, and then tested the ability of VLPs to bind to 4G2 by ELISA (Figure 3.5A). Of the selectants, three exhibited strong binding to 4G2. All had the same peptide insert, NWDPTQFPGK (Figure 3.5B). This peptide has no obvious sequence homology to the amino acids that have been implicate in the AMA1 4G2 epitope (Figure 3.4).

We next investigated the immunogenicity of the 10mer selectant by immunizing groups of Balb/C mice 2 times with 10ug VLPs (10mer selectant or wild type MS2 VLP control) at a 2-week interval. Two weeks after the second dose, peptide-specific and recombinant AMA1-reactive IgG titers were measured by ELISA (Figure 3.6). In order to measure peptide-specific responses, we constructed a PP7 VLP that displayed the NWDPTQFPGK peptide and used it as the ELISA target antigen. Mice immunized with the 10mer selectant VLP had high-titer peptide-specific responses (10^4-10^5) (Figure 3.6A). However, only a subset (3 of 10) of the mice immunized with the 10mer selectant VLPs elicited low-titer antibodies that cross-reacted with recombinant AMA1 (Figure 3.6B, 'responders'). The majority of mice immunized with the selected VLPs were 'non-responders', in that they failed to elicit AMA-reactive antibodies. All of the immunized mice, including 'non-responders', had similarly high peptide titers, so we could not attribute the variable response to gross quantitative differences in the antibody responses in individual mice. We considered the possibility that mice have a low frequency of B cells that are capable of producing AMA-reactive antibodies. However, the use of higher doses of antigen (25μg) also failed to increase the percentage of 'responders' (data not shown).

To better characterize the differences between 10mer selectant VLP-immunized AMA1-responders and non-responders, we boosted immunized mice with 25μg of recombinant AMA1 protein and compared antibody responses to mice that were only immunized with the AMA1. Figure 3.7 shows the subsequent peptide-specific responses in these groups of animals. Immunization with AMA1 alone elicited no peptide-specific response, and there was no boost in peptide titers seen in the group of non-responders. The initial responders, however, were observed to have a detectible peptide-specific IgG boost in response to AMA1 vaccination. This may be an indirect indication that we elicited 4G2-like antibody responses in a subset of animals, and that these animals were able to respond to a boost with the native antigen of 4G2 (AMA1). In order to verify this, we tested the ability of our immune sera to compete with 4G2 for binding to AMA1. While we observed no 4G2 competitive ability in serum from mice immunized with MS2 VLPs, we did see a 2.5-fold difference between sera dilution able to inhibit 50% binding of 4G2 to AMA1 in the AMA1-boosted responders (1:100) as compared to AMA1-boosted non-responders (1:40) (Figure 3.8). AMA1-boosted non-responder sera also seemed to compete better than AMA1-only immune sera, which inhibited 50% of binding at a 1:20 dilution.

Based on previous experience with affinity selections, we had anticipated seeing families of selected peptides in the final round of the 10mer VLP selection. Because there was so little homology in final selectants and only one high-affinity clone was identified, we pursued two additional avenues. First, we reasoned that if we had found the only sequence of a theoretical family of peptide mimotopes for 4G2 that

happened to not be represented in the first 10mer selection, we could recreate the family and repeat the 4G2 selection. In this way we might potentially improve upon the variable immunogenicity of our original 10mer selectant by finding a mutagenized sequence that acted as better mimotope. Secondly, we asked whether 4G2 mimotopes might be better represented as different-length peptides that 10mers. We therefore also performed 4G2 affinity selection using a mixed library with 6, 7, 8 and 10mers insert VLPs represented. In both of these strategies, we performed deep sequencing at each round to shed more light on the types of peptides being selected and potential vaccine candidates worth pursuing.

Affinity selection using a mutagenic library based on the 10mer selectant. A library of recombinant VLPs based on the original 10mer selectant was generated by randomizing the nucleotide sequence encoding the peptide insert. This was achieved by mutagenic primer design utilizing weighted mixes of nucleotides at each of the 30 positions (76% original nucleotide and 8% each other nucleotide). The rationale for this proportion was that even in a relatively low-diversity 10^6 library we would be able to detect the original sequence, which should represent 0.018% or ~1,800 copies. This bore out in our deep sequencing of the library, which yielded the correct proportions of nucleotides (Table 3.1 shows the first 6 nucleotide positions) as well as 0.12% representation of the original sequence, out of our 10^7 library.

Two rounds of low affinity selection were performed on this library to make it as stringent as possible, since there was already a known high-affinity binder in the

population (the original 10mer). Figure 3.9 compares 4G2 capture ELISA data from the final 10mer selectant library with all rounds of the mutagenic library selection, in which a rapid increase in average affinity of the pooled VLPs is seen. Unsurprisingly, even the original (un-4G2-selected) library exhibits above-background binding. Deep sequencing from all rounds of 4G2 affinity selection are shown in Table 3.2. An assortment of peptide selectants have been highlighted so they can be tracked across the selection. The original 10mer clone remained the most represented by number of reads total in each round, however fold-enrichment was much greater for other selectants (%total in one round divided by %total in preceding round). Underlined peptides were selected to test further for immunogenicity.

Affinity selection using a mixed insert-length VLP library. To address our second concern, that 4G2 mimotopes may be better identified from a more length-diverse library of recombinant VLPs, we performed 3 rounds of affinity selection with a mixed library of VLPs displaying 6mers, 7mers, 8mers, and 10mers. We performed one round of selection at high valency, and two rounds at low-valency. The enrichment of 4G2 selectants is shown in Figure 3.9. By the end of round 2, significant 4G2-binding was seen above background, and very high average affinity of the final pool of selectants was seen after the third (final) round. Deep sequencing data from the final round of mixed library affinity selection is shown in Table 3.3. Within the top ~1,450 unique selectant sequences, 9 families (of more than 10 members) were identified. Bold sequences represent the highest ranked peptide within the family based on total reads at the final round, and shaded cells contain

the consensus sequence for each family. It is noteworthy that the VTHDAWRPD selectant is a 9mer, which was not intentionally represented in the original mixed library. While the presence of codon insert or deletion errors aren't surprising in the context of iterative amplification in affinity selection [37], it was interesting that a presumably rare mistake would have been selected for. Underlined peptides in Table 3.3 were chosen to test for immunogenicity. Fold-enrichment was taken into consideration, which is shown in Table 3.4 for top-ranked family members. Because we don't have deep sequencing data for the original mixed-length libraries, it isn't possible to address how much enrichment occurred after one round of sequencing for this selection.

Characterization of selectants. Plasmids encoding nine of the new VLP selectants (listed in Figure 3.10B) were constructed, verified by sequence analysis, then used to generate VLPs. Figure 3.10A shows the electrophoretic mobility of the VLPs on an agarose gel compared to wild type MS2 VLPs. By 4G2 end-point dilution titering, we were able to roughly compare affinity of the three mutagenic VLPs with the original 10mer (Figure 3.11A). While they are each bound at fairly low concentrations of 4G2 ($\sim$1:10^4), it is worth pointing out that the NWDPIQFPGK clone is the lowest-affinity of the group (by $\sim$10 fold). In general, the VLPs from the mixed library selection also showed strong binding to 4G2, but two selectants from one family (VTHDGLEGQM and VTHDAWRPD) bound 100-1000 fold less than other selectant VLPs.

Each of these VLPs was used to immunize groups of Balb/C mice (three times with

5ug VLP in 50% IFA, at 2-week intervals) and AMA-1 antibody responses were measured by ELISA (Figure 3.11B). Surprisingly, the weakest 4G2 binder (VTHDAWRPD) elicited the most consistent AMA1 cross-reactive IgG responses. Most of the other VLPs failed to elicit anti-AMA1 antibodies, although one of the selectants from the mutagenic library (NWDPIQFPGK) also elicited low titer antibody responses to AMA1 in a majority of immunized animals. To summarize these studies, the VTHDAWRPD- and NWDPIQFPGK-displayed VLP selectants represent two examples of low affinity binders that seem to perform the best as 4G2 mimotopes.

Discussion

We have approached the problem of identifying vaccine candidates for the highly polymorphic *Plasmodium* parasite by screening several types of VLP-displayed peptide libraries. In order to target a specific conserved region of the blood-stage of the parasite, a selecting antibody was chose that is able to broadly bind and neutralize different *Plasmodium* strains [90]. The native epitope is highlighted in Figure 3.4, and includes residues Lys^{351}, Gln^{352}, Phe^{385}, Asp^{388}, and Arg^{389} (from *P. falciparum* sequence), which span a disordered-loop region of the protein. The 4G2 epitope has been defined by myriad studies since the structure of AMA1 from *P. vivax* was first solved, using site-directed mutagenesis and deletion studies of whole domains as well as individual amino acids [21, 74, 87]. It is likely that 4G2 grants its neutralizing activity by binding in close proximity to a highly conserved hydrophobic trough on AMA1 that is directly involved in erythrocyte invasion-

critical interactions [22, 91]. This is either due to occlusion of the binding site or prevention of necessary conformational changes that facilitate the interaction [19].

Our selections yielded VLP selectants that shared no obvious homology to the 4G2 epitope on AMA1. Sequence homology between native epitopes and mimotopes is not necessarily expected, as the molecular interactions that define binding of antibody to either native antigen or structural mimotope occur at the atomic level rather than the amino acid level. As a preliminary criterion for prioritizing selectants, we therefore used relative affinity of individual clones for 4G2.

In the initial 10mer selection, the only clone to meet this condition was tested for immunologic mimicry. The variable AMA1 cross-reactive responses seen upon immunization indicated that this clone acted as a relatively poor mimotope. A multitude of past studies are reminiscent of these results, and have shown poor or variable immune responses to mimotopes initially identified as the highest affinity binders [36, 97, 98]. We addressed the question of whether our selectant could be improved as a mimotope by randomizing the VLP-displayed sequence and repeating affinity selection with 4G2. In this selection we also performed deep sequencing of the selected peptides at each round, and pursued immunogenicity studies based on fold enrichment throughout the selection. One mutagenic selectant in particular was characterized by strong enrichment (NWDPIQFPGK), but did not bind more strongly to 4G2 as compared to the original 10mer selectant. Although antibodies elicited by this VLP bound only weakly to AMA1, all three mice immunized elicited cross-reactive antibodies.

These results were somewhat mirrored in the mixed library 4G2 selection. By sorting selectants into sequence families and investigating the most enriched or top-ranked family members for immunogenicity, we were able to identify another VLP selectant (VTHDAWRPD) that bound poorly to 4G2 but consistently elicited AMA1 cross-reactive antibodies. It may be significant that this VLP clone exhibited the most enrichment in the low valency (Table 3.4), low selecting antibody (third) round of selection, which is the most stringent for competition and limiting avidity effects. To address the diversity of families of selectants we identified in the final round, it seems likely that they bind separate paratopes in the antigen-binding site of the selecting mAb. In this way, selectant VLP families may be seen to have high affinity but may use separate molecular contacts to bind the mAb than the native antigen, and these would not act as mimotopes or be expected to elicit the antibody response similar to the native Ag. Our mixed library affinity selection data would suggest that it is important to investigate many families represented as selectants, even those that may exhibit limited binding to the selecting antibody such as the VTH group of sequences.

Although the two VLP selectants from the mutagenic and mixed library selections seem to be improved mimotopes, they are unlikely to be protective used on their own as vaccines given the low titers of AMA1 response they elicited. As we showed previously with the 10mer selectant however, a pre-existing low-level of immune cross-reactivity may grant a strong 4G2-like immune response if a recombinant AMA1 protein boost is given in a VLP prime/AMA1 boost immunization scheme. This type of strategy might circumvent the issues of antigenic variation seen in the

recent Phase 2 clinical trial utilizing a strain-specific AMA1 protein [84]. Recombinant AMA1 from almost any *Plasmodium* species or strain contains the conserved 4G2 epitope, and would presumably boost a pre-existing 4G2-like response similar to what we observed with the original group of 10mer-immunized responders (Figures 3.7-8) [85]. This finding may have therapeutic implications as well. During the course of natural infection a 4G2-like response might be generated more rapidly if a pre-existing pool of partially cross-reactive B cells was available for boosting, targeting the immune response to the neutralizing (but normally immunosubdominant) 4G2 epitope [36]. The evidence that the 4G2 epitope is highly conserved indicates that it is not under strong immune pressure and/or is located in a critical region for parasite survival [75]. From what has been revealed in recent studies, it seems that both mechanisms are probably responsible for conservation [19, 21]. With the proper stimulation however, B cells might more efficiently target the 4G2 epitope, and it seems unlikely that AMA1 (and the parasite as a whole) could afford escape mutations at this site.

As immediate future directions, there are several as-yet untested peptides identified in these affinity selections that seem promising. From the mutagenic selection, the very high enrichment observed after only one round of selection with the NWDPAKFPGK clone is intriguing (Table 3.2, in maroon). Also, the remaining family members of the VTH group of selectants may provide an even more immunogenic mimotope than the one identified here. These 4G2 mimotope VLPs may contribute to malaria vaccine strategies in the future. More generally though, the strategy we used has allowed direct progression from a) mAb affinity selection to b)

characterization and prioritization of selectants by deep sequencing to c) immunization with VLP selectants. Eventually, we may be able to draw broader conclusions about affinity selections through these types of studies. For example, to better understand how to prioritize affinity selected vaccine candidates in the future. We have described several unexpected examples of low affinity selectants acting as the most highly immunogenic mimotopes. Future work will hopefully reveal if this is a characteristic of 4G2 itself or mAbs that recognize conformational epitopes in general.

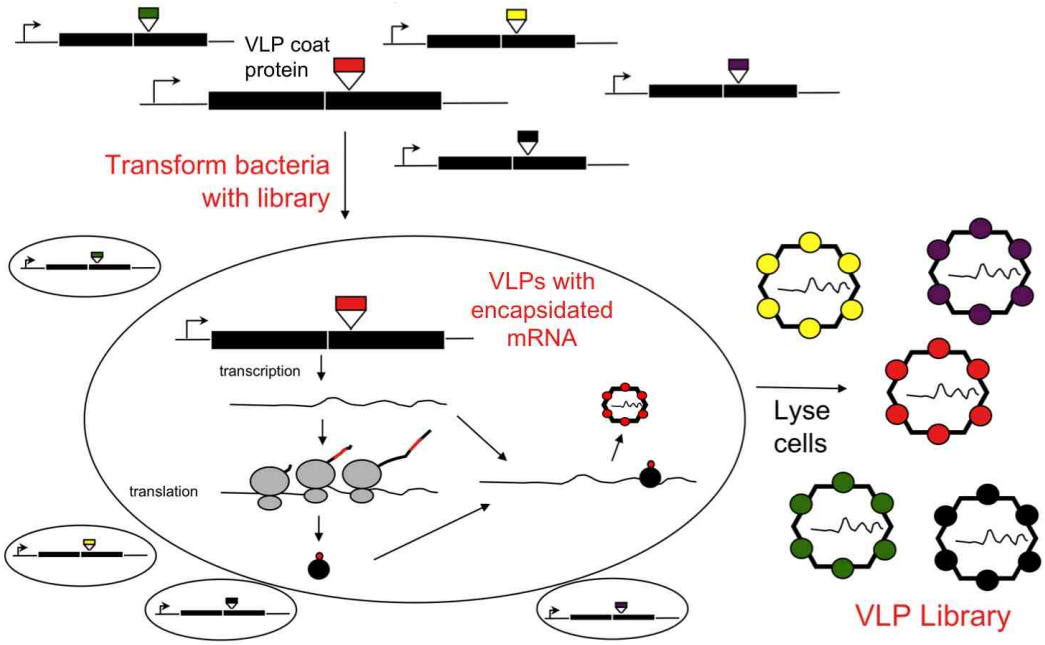

Figure 3.1. Use of a diverse plasmid library to generate a recombinant VLP library. *E. coli* were transformed with a library of plasmids encoding an insert-tolerant single-chain dimer version of the MS2 coat protein. Each coat protein dimer contains a unique peptide insert sequence (represented by a colored rectangle at upper left) resulting in display of the peptide sequence in a surface-exposed AB loop of the formed VLP (1 peptide insert per dimer; 90 dimers per VLP; colored circles at lower right). Each VLP encapsidates its encoding mRNA, including the heterologous peptide sequence.

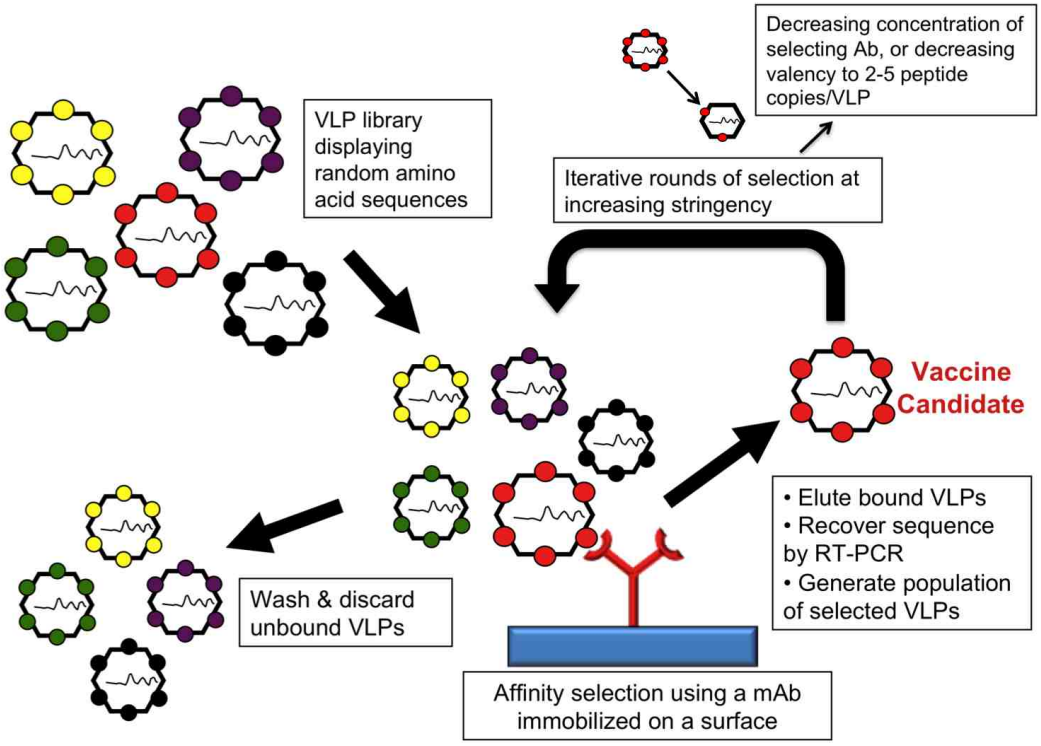

Designations for independent selections	Type of VLPs used as starting library	Valency (and amount 4G2 used) at each round: 1	2	3	4
10-mer	High valency 10-mer peptide insert VLPs	High (250ng)	High (250ng)	Low (250ng)	Low (50ng)
Mutagenic	Low valency 10-mer peptide insert VLPs; mutagenesis based on a 10-mer selectant from the above selection	Low (250ng)	Low (50ng)		
Mixed	High valency 6-, 7-, 8- and 10-mer insert VLPs (mixed equal quantities of each)	High (250ng)	Low (250ng)	Low (50ng)	

Figure 3.2. Affinity selection using immobilized monoclonal antibody. A diverse (~10^{10}) library of recombinant VLPs is iteratively passed over immobilized selecting antibody, in this case 4G2. Recovery of binders by washing then elution is followed by amplification of selected recombinant VLPs by using the encapsidated encoding mRNA as a template for RT-PCR and PCR. Stringency of the selection is increased in later rounds by decreasing the amount of immobilized antibody and/or decreasing the valency of display of heterologous peptide antigen. Specific descriptions of the three affinity-selections performed are noted in the chart.

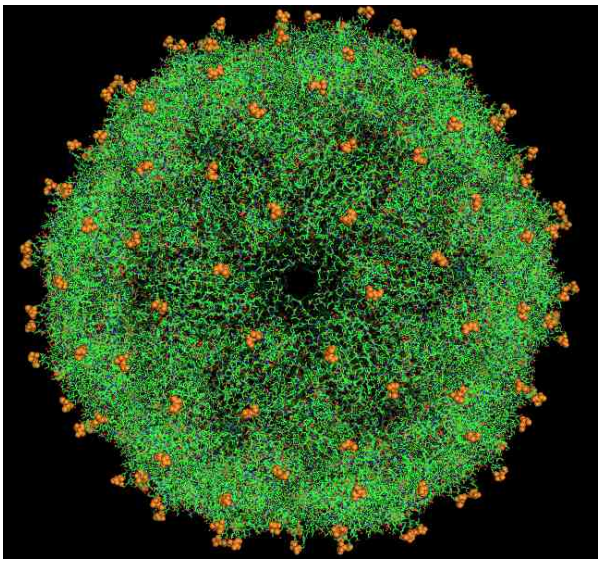

Figure 3.3. Crystal structure of the bacteriophage MS2 VLP. The surface exposed AB-loops of MS2 coat protein are highlighted in orange. This was the site of insertion used to generate libraries of recombinant VLPs used in affinity selection. This image was generated using the coordinates provided by the VIPER database using the program PyMOL.

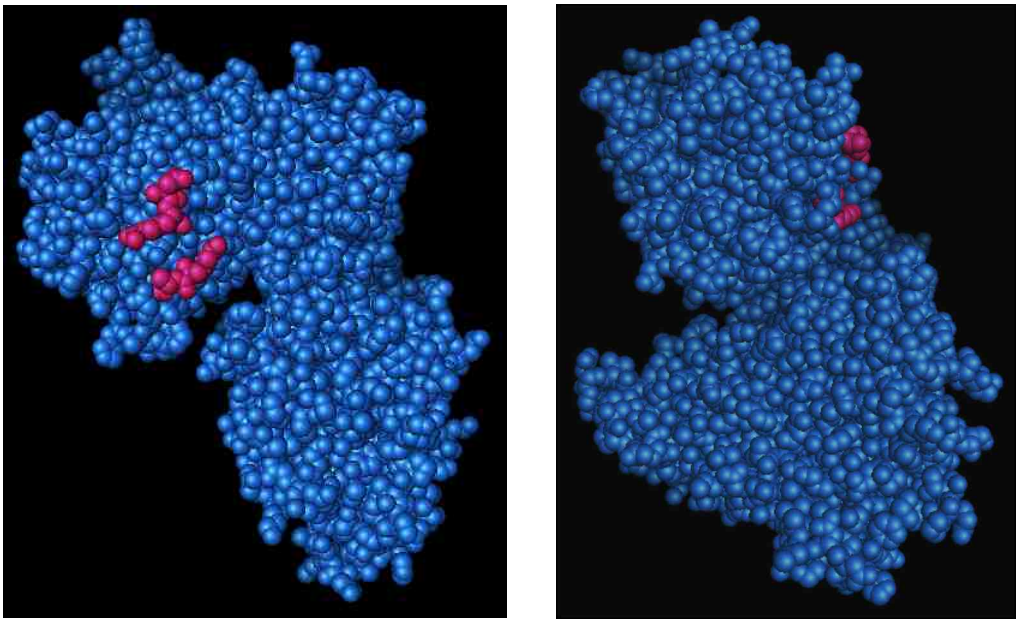

Figure 3.4. Crystal structure of the AMA1 protein from *Plasmodium falciparum*. The putative 4G2 epitope is highlighted in magenta (Lys^{351}, Gln^{352}, Phe^{385}, Asp^{388}, and Arg^{389}); 2 views are provided. These images were generated using the coordinates provided by the RCSB protein data bank using the program PyMOL.

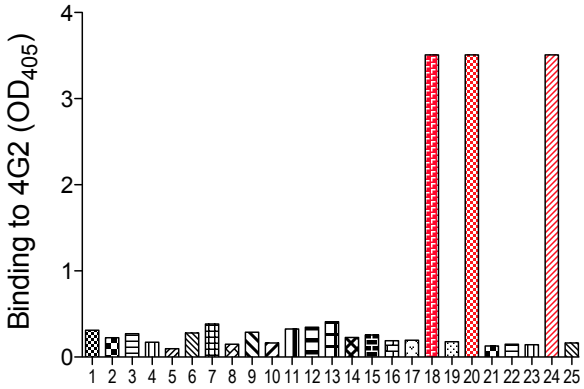

A

	Sequence of clones used in ELISA
1	G G G P G P H R R G
2	L I S D W P V A P E
3	H K G H Y Q G P V Y
4	I V I L G Q L P P T
5	A A F M N I P D G T
6	E G E G P G R R Y A
7	A E P W A M T C G E
8	C S V S A M P D G S
9	D I R N L R M H L K
10	V E H Q P K V A G V
11	K T Y S P S L V A S
12	L P R L D R D S N Q
13	M H Q G P T G N S S
14	N M P V N S G R Y D
15	G W Y G T G G P G S
16	T Y R C V G E D P S
17	P G R T S R A R R W
18	**N W D P T Q F P G K**
19	F A E L P G D N N G
20	**N W D P T Q F P G K**
21	Q G S Q G L S P Q N
24	**N W D P T Q F P G K**
25	Wild type MS2 control

B

Figure 3.5. 4G2 capture ELISA for detection of 4th round 10-mer VLP selectants. Individual affinity-selected recombinant VLP clones were screened by capture using immobilized 4G2 (A), then sequenced (B). The clone highlighted in red exhibited the only strong binding seen above background (wild type MS2 control, on the far right of graph in B).

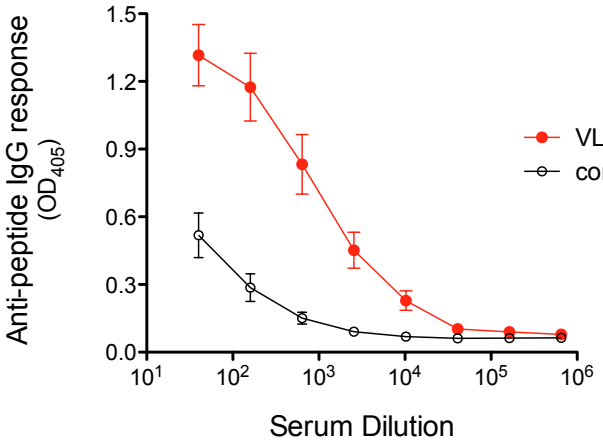

A

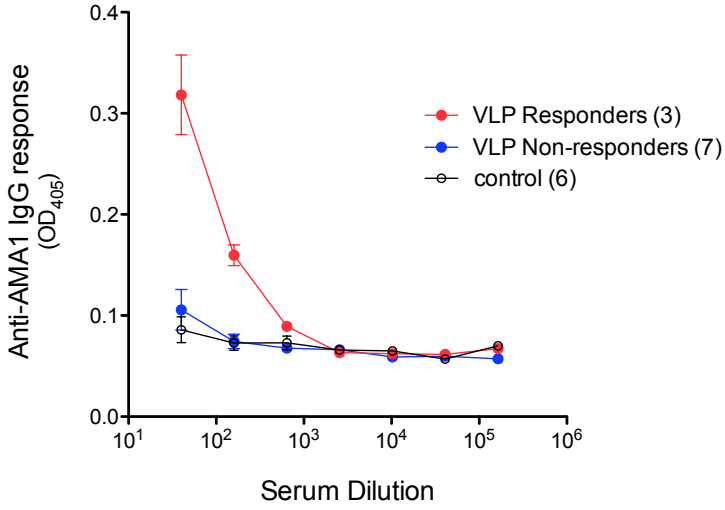

B

Figure 3.6. High peptide-specific and variable AMA1-reactive IgG titers achieved by two immunizations with a selectant VLP. Vaccine-elicited peptide titers were assessed using recombinant PP7 bacteriophage VLPs displaying the NWDPTQFPGK peptide (in a surface-exposed AB loop similar to that of MS2) as the target in an end-point dilution ELISA (A). AMA1-reactive titers are shown for 10 total animals that exhibited variable cross-reactivity with the native antigen of 4G2; in 3 animals, low-titer but positive cross-reactivity was observed (these are termed 'responders'), in contrast to the remaining seven mice ('non-responders') (B). Control refers to wild-type MS2-immunized mouse sera. Immunizations with recombinant and wild-type VLPs consisted of two 10ug doses given at a 2-week interval, and AMA1 immunization consisted of one 25ug dose with 50% IFA. Mean and SEM are shown, and the numbers of mice in each group are noted in parentheses.

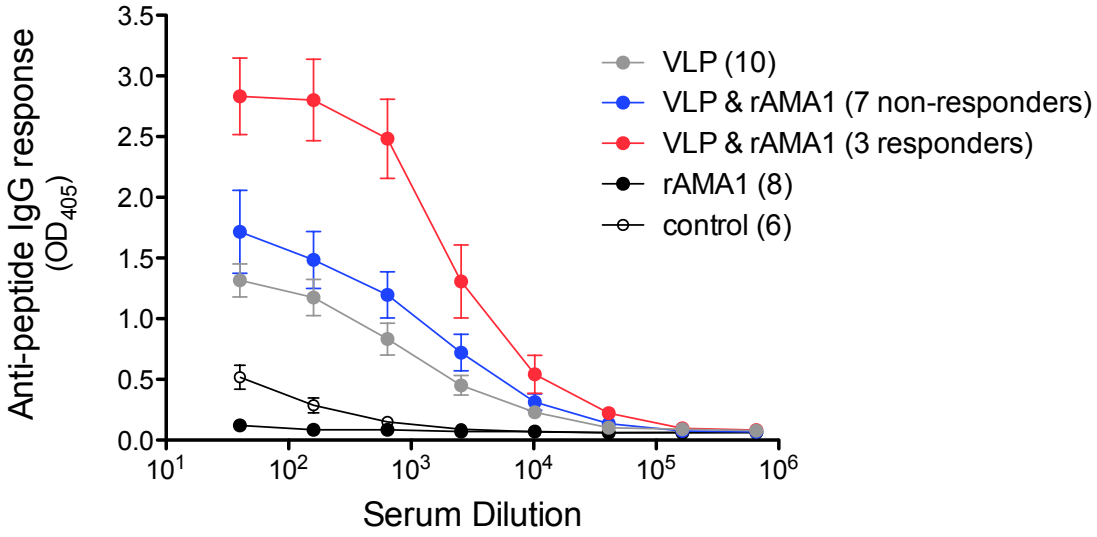

Figure 3.7. Immunization with recombinant AMA1 boosts anti-peptide titers only in 'responders'. Animals that had AMA1-cross-reactive titers present after VLP-selectant immunization were boosted by AMA1 (red line compared to grey) in contrast to animals that did not respond to VLP immunization (blue line compared to grey). Control refers to wild-type MS2-immunized mouse sera. Immunizations with recombinant and wild-type VLPs consisted of two 10ug doses given at a 2-week interval, and an AMA1 boost consisted of one 25ug dose with 50% IFA. Mean and SEM are shown, and the numbers of mice in each group are noted in parentheses.

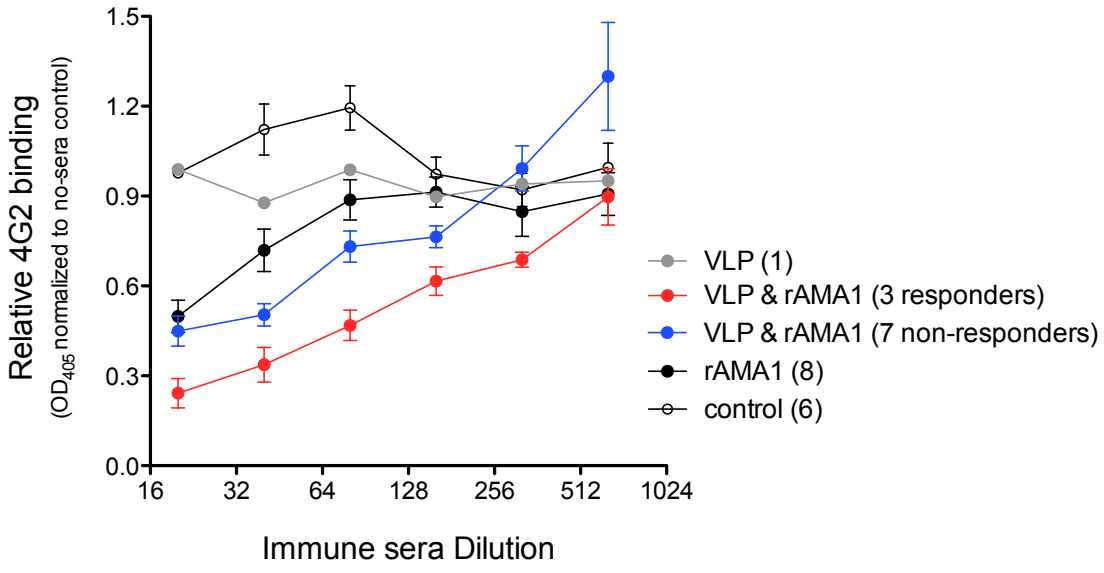

Figure 3.8. Competition of immune sera with 4G2 for AMA1 binding. Sera from animals with AMA1 cross-reactivity after VLP immunization ('responders', red) is more competitive with 4G2 (1:20,000) for AMA1 binding than other sera. Control refers to wild-type MS2-immunized mouse sera. Immunizations with recombinant and wild-type VLPs consisted of two 10ug doses given at a 2-week interval, and an AMA1 boost consisted of one 25ug dose with 50% IFA. Mean and SEM are shown, and the numbers of mice in each group are noted in parentheses.

Table 3.1. Verification of mutagenic plasmid library composition. Primers used for site-directed mutagenesis were designed by randomization of the nucleotide sequence encoding the high-affinity 4G2 selectant NWDPTQFPGK (AAC TGG GAC CCG ACC CAG TTC CCC GGC AAG). Each of the thirty nucleotide positions in the mutagenic library was weighted for 76% chance of resembling the original nucleotide, or 8% chance of each other nucleotide. Percent occurrence of nucleotides was determined by deep sequencing of the plasmid library.

Nucleotide position	Percent occurrence of nucleotides at each position: **A**	**G**	**C**	**T**
1 (A)	78.716	7.047	6.139	8.098
2 (A)	78.768	7.612	6.360	7.260
3 (C)	8.965	7.408	75.114	8.513
4 (T)	9.081	7.037	8.014	75.868
5 (G)	10.541	73.913	6.826	8.721
6 (G)	10.177	73.874	6.927	9.022

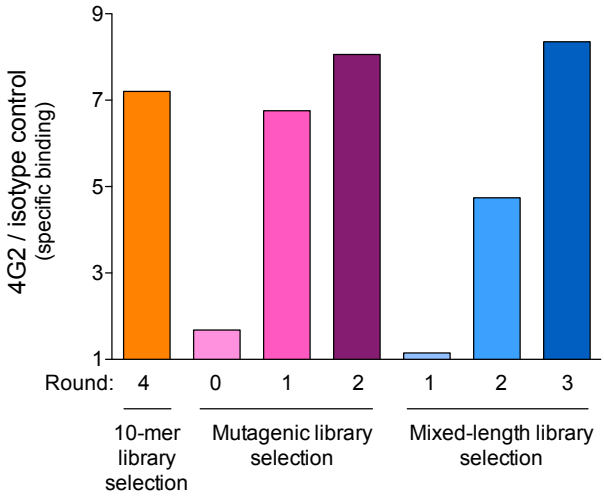

Figure 3.9. 4G2 *vs*. isotype antibody capture ELISA for detection of VLP library binding (an estimate of library affinity) at each round of affinity selection. The orange bar represents the final library from a selection using only a 10-mer insert VLP library (i.e. the library from which NWDPTQFPGT was identified). The pink bars represent all the stages of selection, including the original mutagenic library (round 0), using a VLP library with insert sequences randomized from the 10-mer NWDPTQFPGK selectant. The blue bars represent the stages of a selection in which 6-, 7-, 8- and 10-mer VLP libraries were mixed together prior to 4G2 affinity selection. Representative capture ELISA results are shown of three dilutions of each library that were examined for binding to 4G2 and isotype, and in which the same trends were observed.

Table 3.2. Top ~40 peptides from the each round of 4G2 affinity selection using a mutagenic library based on the peptide shown in the shaded row. Fold enrichment of peptides was calculated by dividing % total of the current round by the previous round % total. Coloring allows comparison of enrichment across the selection, and underlined peptides were further tested for immunogenicity.

Round 2 peptide selectants	Reads	% of total	Fold enrichment	**Round 1** peptide selectants	Reads	% of total	Fold enrichment	**Original** mutagenic library	Reads	% of total
NWDPTQFPGK	12115	8.180	77.98	NWDPTQFPGK	1511	2.168	20.66	NWDPTQFPGK	99	0.105
NWDPIQFPGK	12049	8.136	548.39	NWDPIQFPGK	890	1.277	86.06	KWDPTQFPGK	34	0.036
NWDPIKFPGK	7310	4.936	132.34	NWDPTQYPGK	766	1.099	69.13	NWDPTQLPGK	32	0.034
NWDPTKFPGK	6599	4.456	210.24	NWDPTQFPDK	681	0.977		NRDPTQFPGK	30	0.032
NWDPNQFPGK	5653	3.817	4.01	NWDPNQFPGK	664	0.953	56.18	NWDPTQFPGN	25	0.026
NWDPAKFPGK	5505	3.717	5.88	NWDPTKFPGK	605	0.868	40.95	NWEPTQFPGK	25	0.026
NWDPTQYPGK	5340	3.606	3.28	NWDPAKFPGK	441	0.633	597.0	NLDPTQFPGK	24	0.025
NWDPVKFPGK	4284	2.893		KWGQTALPDM	395	0.567		NWDPTKFPGK	20	0.021
NWDPTRFPGK	3684	2.487	4.88	KWDATWFPVN	392	0.562		NWDTTQFPGK	19	0.020
NWDPNKYPGK	3266	2.205		NWNPTQFPGK	369	0.529	27.75	NCDPTQFPGK	18	0.019
NWDPAQFPGK	2962	2.000		NWDPTQFPGY	368	0.528		NWDPSQFPGK	18	0.019
NWDPTKFPGM	2286	1.544		NWDSTQFCGN	361	0.518		NWDPTQFPRK	18	0.019
NWDPSQFPGK	1988	1.342		NWDPTRFPGK	355	0.509	43.69	NWDPTQFSGK	18	0.019
NWDPARYPGK	1760	1.188		NWKPIQLPGT	339	0.486		NWDPTQIPGK	18	0.019
NWDPTQYPGM	1641	1.108		SQDPTQYSDK	335	0.481		NWNPTQFPGK	18	0.019
NWDPAKYPGK	1634	1.103		NSVPSQYSGK	332	0.476		NGDPTQFPGK	17	0.018
NWDPTRYPGK	1602	1.082		NWGPNKFPGK	324	0.465		NWDPTHFPGK	17	0.018
NWDPKQFPGK	1537	1.038		TWHPSQFHGM	321	0.460		NWDPTQFPGT	17	0.018
NWDPIQFPGM	1399	0.945		IYYQTTFSGY	319	0.458		NWDPTQVPGK	17	0.018
NWDPSKFPGK	1393	0.941		NWDPTQYPGL	319	0.458		NWDLTQFPGK	16	0.017
NWDPTQFPGM	1235	0.834		NWDPAQFPGK	314	0.450		NWDPNQFPGK	16	0.017
NWDPIQFPGR	1107	0.747		NWDPIQFRGK	314	0.450		YWDPTQFPGK	16	0.017
NWDPIQYPGK	1082	0.731		NWDPSQFPGK	302	0.433		NWDPTQSPGK	15	0.016
NWDPTQYPGL	1028	0.694		IGDPRQCSVQ	295	0.423		NWDPTQYPGK	15	0.016
NWDPVQFPGK	1013	0.684		NWNPTLYQYM	292	0.419		SWDPTQFPGK	15	0.016
NWDPNQFPGM	997	0.673		HWADTQFHRT	283	0.406		NSDPTQFPGK	14	0.015
NWDPNQYPGK	954	0.644		NWDQNKFPGM	281	0.403		NWDPIQFPGK	14	0.015
NWDPTKYPGK	914	0.617		NWDPTQCTTN	270	0.387		NWDPTQFPDK	14	0.015
NWNPTQFPGK	880	0.594		HLDHTDLPSK	259	0.372		TWDPTQFPGK	14	0.015
NWDPSEFPGK	870	0.587		NWDTTQFPDK	257	0.369		IWDPTQFPGK	13	0.014
NWDPTQFPGQ	751	0.507		NWDPTDIPGK	249	0.357		NWDPTLFPGK	13	0.014
NWDPSQYPGQ	632	0.427		NCVPIQLFRK	247	0.354		NWDPTQFPCK	13	0.014
NWDPIKFPGY	622	0.420		TWDPPQVPGK	247	0.354		NWDRTQFPGK	13	0.014
NWDPDRFPGK	604	0.408		RGDQTQFLGK	243	0.349		NWDSTQFPGK	13	0.014
NWDPCQFPGK	584	0.394		NGNPTQVPCE	223	0.320		NWHPTQFPGK	13	0.014
NWDQNKFPGM	584	0.394		NRVPTKIHDR	223	0.320		HWDPTQFPGK	12	0.013
NWDPYKFPGK	541	0.365		NWDPTEYPCK	220	0.316		NWAPTQFPGK	12	0.013
NWDPRRFPGK	515	0.348		NWDPTQFPGM	220	0.316		NWDPTQFAGK	11	0.012
GWDPLKFPGK	502	0.339		TSDSTQCAGK	220	0.316		NWDPTQFLGK	11	0.012
…				…				…		
				NWDPIKFPGK	26	0.037	35.20	NWDPTRFPGK	11	0.012
								NWDPIKFPGK	1	0.001
								NWDPAKFPGK	1	0.001

Table 3.3. Families of peptides from the 3rd (final) round of 4G2 mixed-library affinity selection. Peptides in shaded boxes represent family consensus sequences, and bold peptides represent the highest-ranking members of each family (with the rank number noted). Underlined peptides were tested for immunogenicity.

	RVSRRGGP	GPGRMR	PGDHRSA	PGEMERA	IEHGPVA	PGHPRRG	VTHDALEGQM	ASAAGRA
1	ALSAGGP	GAGQMR	HGDHRSA	PADDEAA	IEHEPVA	PGHLRRG	DHARRLEGQM	ASAAGGP
2	AVSAGGP	GAGRMR	LGDHRSA	PAYDEAA	**IEHGPVA (37)**	PGHPRRG	VTARRLEGQM	ASAAGRP
3	HVSAGGP	GPGQMR	**PGDHRSA (1)**	PGDDEAA	IEHGPAA	PGPLRRG	VTHDRLEGQM	ASAPGGP
4	RVSAGGP	GLGRMR	RGDHRSA	PGDDERA	IEHGPIA	**PGTLRRG (10)**	VTHGRLEGQM	RSAAGGP
5	RVSAGG	GPGRMR	SGDHRSA	PGRDEAA	IEHGPVG	PRHLRRG	VTHDALEGQM	SSAAGGP
6	RVSAGGA	GQGRMR	TGDHRSA	PGADERA	IEHGPVR	PGHPARG	VTHDAWEGQM	ASAAGRA
7	RVSAGGPG	**GRGRMR (3)**	PADHRSA	PGEDERA	IERGPVA	PRHPARG	VTHDGLEDQM	HSAAGRA
8	RVSAGGR	GSGRMR	PADHSSA	PGRDERA	IEHGPRR	PGTPRRG	**VTHDGLEGQM (91)**	RASAAGRA
9	RVSAGRP	RAGRMR	PADTRSA	PGVDERA	IEHGAHR	PGTLRRGG	VTHDGLEGQT	**RSAAGRA (296)**
10	RVSPGGP	GPGGMR	PAHHRSA	PGRDRAA	IEHGARR	PRYLRRG	VTHDGLGGQM	RSAPGGP
11	RVSRGGP	GPAGMR	PATHRSA	PGRHEAA		PGHPAAGG	VTHDRLGGQM	RSAPGRP
12	RVSRGG	GPGRMC	PAYHRSA	PAEDERA		PRHPAAGG	VTHDSLEGQM	RAQAAGRA
13	RVSAGRA	GPGRTR	PCDHRSA	PGEIERA		PRHPAAG	VTHGALEGQM	RARAAGRA
14	RVSAGSA	GPGRVR	PDDHRSA	PGEMERA			VTHGGLEGQM	RGSAAGRA
15	RVSAGRAR	GPSRMR	PRDHRSA	PGESERA			VTHNGLEGQM	RSAAGRAQ
16	RVSAGRV	HRYSGPGRMR	PSDHRSA	PGETERA			VTRDGLEGQM	RGRAAGRA
17	RVSRGRA	RPGRMR	PDNHRSA	PGEYERA			VTHDAWGGQM	RGRRAGRA
18	RVSRGRP	GRARMR	PGDDRSA	PGEIRRA			VTHDAWRGQM	
19	RVSAGRGR	GRVRMR	PGDDRSP	PGEMEAA			VTHDAWEGPD	
20	RVSRGRAR	GSDRMR	PGDDRSV	PGEMERP			VTHDALGGPD	
21	RVSPGRGR	RAGTMR	PGDLRSA	PGEMGRA			VTHDGLEGPD	**PGKPRR**
22	RVSRGRGR	GRAGMR	PGDNRSA	PGEMKRA			VTHDAWRAQM	PGGPRR
23	RVSRGAGR	GSAGMR	PGDPRSA	PGEMMRA			VTHDAWRARW	PGGPRRSA
24	RVSRRRGR	GRAGCR	PGDQRSA	**PGEMRRA (2)**			VTHDGLGGPD	PGKPRR
25	RVSRRRP	RPGTMR	PGDRRSA	PGEMSRA			**VTHDAWRPD (84)**	**PGRPRR (324)**
26	CVSRRAGP	GPAGCA	PGDTRSA	PGEMWRA				PGSPRR
27	CVSRRAGR	GPAGCC	PGDYRSA	RGESERA				RGGPRR
28	CVSRRGGP	GPAGCG	PGDHESA	PGETARA				PGVPRRSA
29	CVSRRVGP	GRAGCA	PGDHESP	PGETEAA				PGKPAR
30	HVSRRAGP		PGDHEVA	PGETERP				PGKAAR
31	RVSRRAGP		PGDHGSA	PGETRRA				PGKPAA
32	HVSRRAGR		PGDHKSA	PAEMRRA				PGRPAR
33	LVSRRAGR		PGDHMSA	PARMRRA				PGRPAA
34	**RVSRRAGR (4)**		PGDHQSA	PATMRRA				RGRPRR
35	VSRRAGR		PGDHSSA	PDEMRRA				REGPRR
36	RVSRRGGP		PGDHWSA	PSEMRRA				PGKAAA
37	RVSRRVGP		PGDRESA	RAEMRRA				PGKARA
38	RASRRAGP		PGGHESA	PARLRRA				PGKPAAG
39	RASRRAGR		PGDTGSA	PARLERA				
	(108 total in family)		*(308 total in family)*	*(68 total in family)*				

Table 3.4. Top selectants from each family of peptides from the 3rd (final) round of 4G2 mixed-library affinity selection. The final rank number for each peptide is noted in parenthesis. Blue-shaded rows highlight peptides tested for immunogenicity.

Mixed-library 4G2 selectants	Enrichment between rounds selection: **1st – 2nd**	**2nd – 3rd**
PGDHRSA (1)	368.64	1.96
PGEMRRA (2)	421.57	1.01
GRGRMR (3)	42.70	0.34
RVSRRAGR (4)	203.08	0.25
PGTLRRG (10)	27.53	0.29
IEHGPVA (37)	1.63	0.49
VTHDAWRPD (84)	1.99	2.50
VTHDGLEGQM (91)	3.15	0.70
RSAAGRA (296)	---	6.29
PGRPRR (324)	27.77	0.36

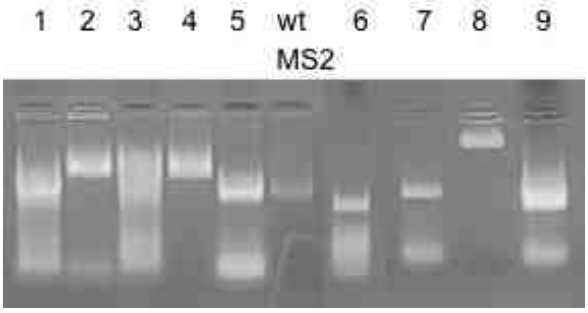

	Insert sequences of selectants
1	P G D H R S A
2	P G E M M R A
3	N W D P I K F P G K
4	N W D P T R F P G K
5	N W D P T Q F P G K
6	N W D P I Q F P G K
7	V T H D A W R P D
8	P G T L R R G
9	V T H D G L E G Q M

Figure 3.10. Purified affinity-selected VLPs displaying 4G2-selected peptides. These clones were identified separately in either the mutagenic or mixed library selections. They were determined to be of interest due to enrichment across the selection (mutagenic selectants, red) or rank within family in the final round (mixed library selectants, blue). Peptide insert was verified by sequencing of each plasmid.

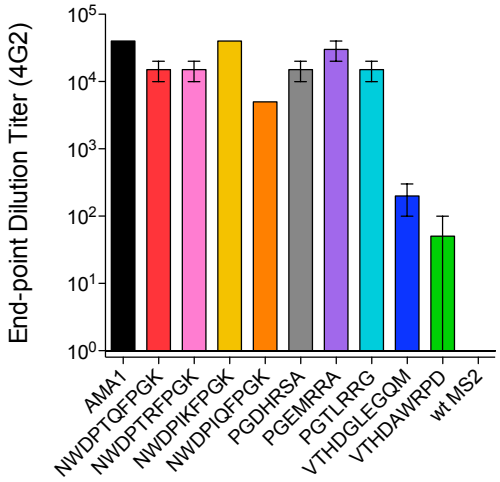

A

Figure 3.11. 4G2-binding and AMA1-specific immunogenicity of VLP affinity-selectants. Panel A shows the end-point dilution of 4G2 reactivity with 500ng of the immobilized VLP target noted under each bar. Panel B shows sera reactivity to 500ng of immobilized AMA1 protein; groups of three mice were immunized 3 times at 2-week intervals, using doses of 5ug VLP with 50% IFA (or 2.5ug doses for NWDPIQFPGK, orange). The insert sequence for the VLP tested is noted in each graph, and 2 promising vaccines are outlined. Mean and SEM are shown for duplicates in A.

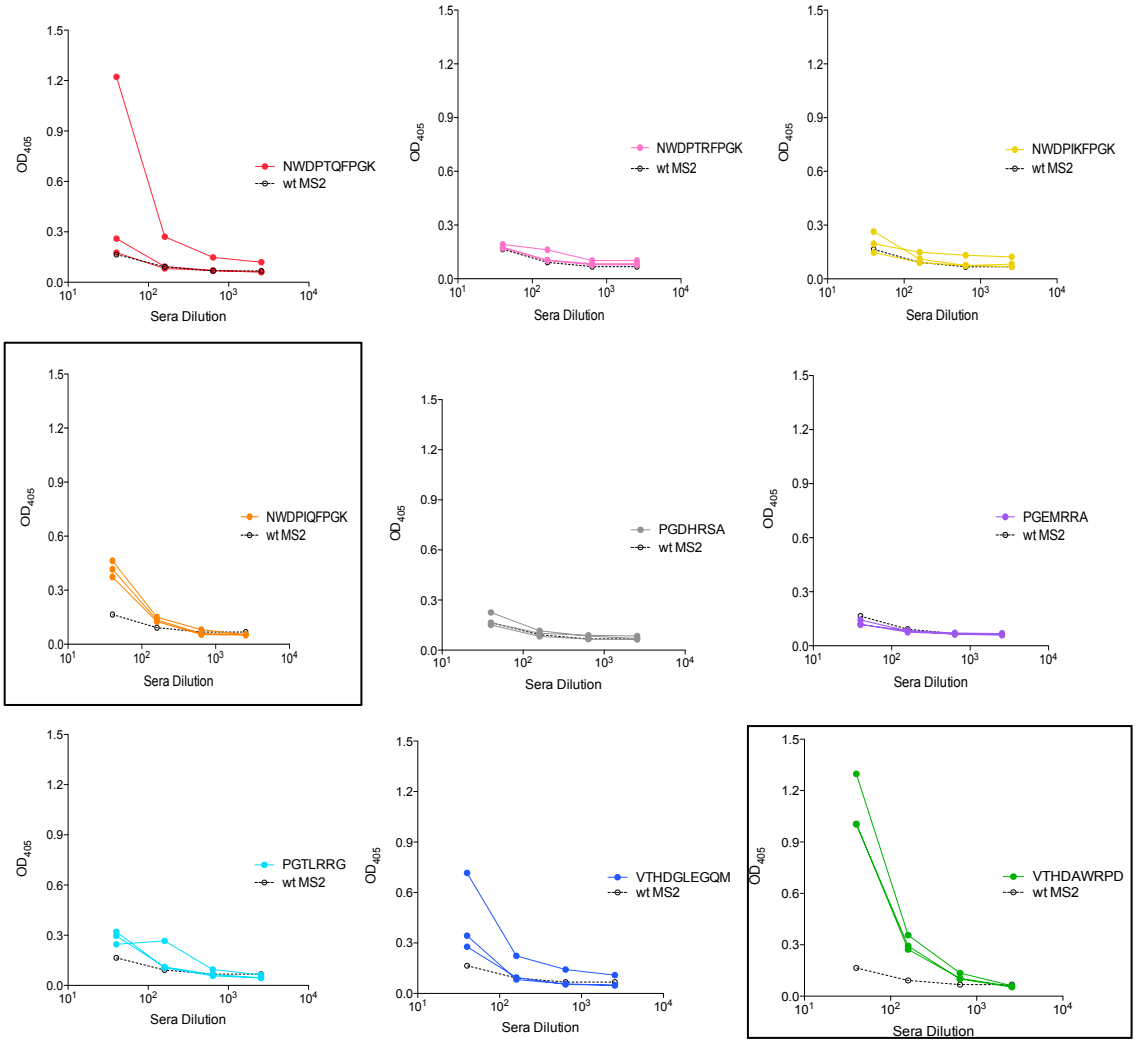

B

Chapter 4: Future Directions and Overview

Future directions with two new targets

In addition to the lipid-lowering and blood-stage malaria parasite vaccine targets that were addressed in Chapters 2 and 3 in depth, we have also investigated the possibility of targeting 2 other proteins, both by rational vaccine design utilizing conjugated Qβ VLPs. The first is a malaria protein that functions in the liver-stage of the parasite life cycle, and the second is a neuronally secreted protein that is specifically phosphorylated in Alzheimer disease.

Circumsporozoite protein (malaria/*P. falciparum* parasite). The first target is the circumsporozoite protein (CSP) of *P. falciparum*, which has been shown to be required for parasite invasion of hepatocytes after sporozoites are transferred to humans from the mosquito vector [99]. The choice of CSP as a vaccine target was based on several lines of evidence. First, CSP was shown to be an immunodominant protective antigen in irradiated sporozoite immunization (an effective but impractical strategy for human vaccination), by observing that immunization was significantly less protective in a mouse model that was tolerant to CSP T cell epitopes [100]. In addition, both antibody and CD4+ T cell responses against CSP were shown to correlate with protection from natural infection in humans [101]. The particular N-terminal CSP epitope chosen for our vaccine was selected due to the high sequence conservation of the N-terminus region of CSP, as well as strong correlation of N-terminal peptide-specific antibody responses with protection in children living in malaria-endemic regions [102, 103]. Lastly, this same CSP N-

terminal region includes a proteolytic cleavage site that is critical in invasion, as treatment with a cysteine protease inhibitor inhibits sporozoite infectivity *in vivo* [104]. Vaccines that target the CSP N-terminus could complement a current leading malaria vaccine candidate RTS,S (which includes some regions of CSP, but not the conserved N-terminal region), and blood stage vaccine candidates such as those we are pursuing in our lab (Chapter 3).

In collaboration with Drs. Amy Noe (Leidos), Gabe Gutierrez (Leidos) and Moriya Tsuji (Aaron Diamond AIDS Research Center), a peptide derived from *P. falciparum* CSP spanning residues 81-95 was constructed with an N-terminal cysteine and 3-glycine spacer, and conjugated to Qβ VLPs using the SMPH chemical crosslinker (as described previously). We immunized a group of 5 Balb/C mice 3 times at 2-week intervals (5ug doses in 50% IFA) and observed high (10^{4-5}), durable (to 6.5 months) peptide-specific and recombinant CSP-reactive IgG titers as compared to wild-type VLP immunized controls (Figure 4.1). We have sent immune and control sera from these animals to collaborators to assess protection from sporozoite invasion of hepatocytes, and have also sent CSP-VLPs to be used in a mouse challenge model in which a transgenic *P. berghei* expressing *P. falciparum* CSP is used [105, 106].

Selectively phosphorylated tau protein (early Alzheimer disease). The second target is Thr_{181}-phosphorylated tau protein (AT270), which is present at elevated levels in cerebrospinal fluid in early Alzheimer disease (AD) as well as related disorders collectively termed tauopathies [107]. It has been proposed that in AD hyperphosphorylated tau undergoes unconventional exosomal release similar to

other aggregation-prone proteins like α-synuclein, prion proteins, and β-amyloid [108, 109]. This may be the cause of the spreading lesions seen in the brain of AD patients, and the cause for pathological neurodegeneration associated with intraneuronal fibrillary tangles (NFTs). A well-characterized mouse model exists in which mutant human tau protein P301L (prone to hyperphosphorylation) is conditionally expressed under a tetracycline-transactivated promoter, such that NFTs develop in cortico-limbic areas of the brain and loss of activity is specifically observed in the forebrain areas that mimic human tauopathies (rTg4150 mice) [110]. Behavioral impairments and neuronal loss are noted as early as 6 months of age in these mice, making this an expeditious experimental model for early AD and tauopathies.

In collaboration with Dr. Kiran Bhaskar and Nicole Maphis, we constructed a peptide derived from human tau protein (residues 492-504) and modified it to include a C-terminal cysteine with a 2-glycine spacer and a Thr_{498} phosphorylation that is hypothesized to be specific to exosomally-secreted tau. We conjugated this peptide to Qβ VLPs using the SMPH chemical crosslinker (as described previously), and immunized groups of Balb/C mice as well as rTg4150 mice 3 times at 2-week intervals (5ug doses in 50% IFA). We have shown that we can elicit high peptide IgG titers in both strains (10^{5+}) as compared to wild-type VLP immunized controls (Figure 4.2). Preliminary behavioral data (including Morris water maze, elevated plus maze and novel object recognition assays performed by Nicole Maphis) indicate improvement in p_{498}Tau-Qβ immunized mice, but studies are ongoing in this model

and we will look at histopathology of brain slices to characterize differences in immunized *vs*. control mice.

Closing Remarks

With these combined studies we have shown the breadth of applications of bacteriophage VLPs, from the development of powerful therapeutic vaccines (targeting PCSK9 for management of cardiovascular disease) to the discovery of novel vaccine candidates (targeting AMA1 in malaria). We have also begun to expand the display capabilities of our VLPs by exploring the use of sortase for specific enzymatic conjugation, and have also identified new vaccine targets (CSP in malaria and phosphorylated tau protein in Alzheimer Disease) that we will continue to develop.

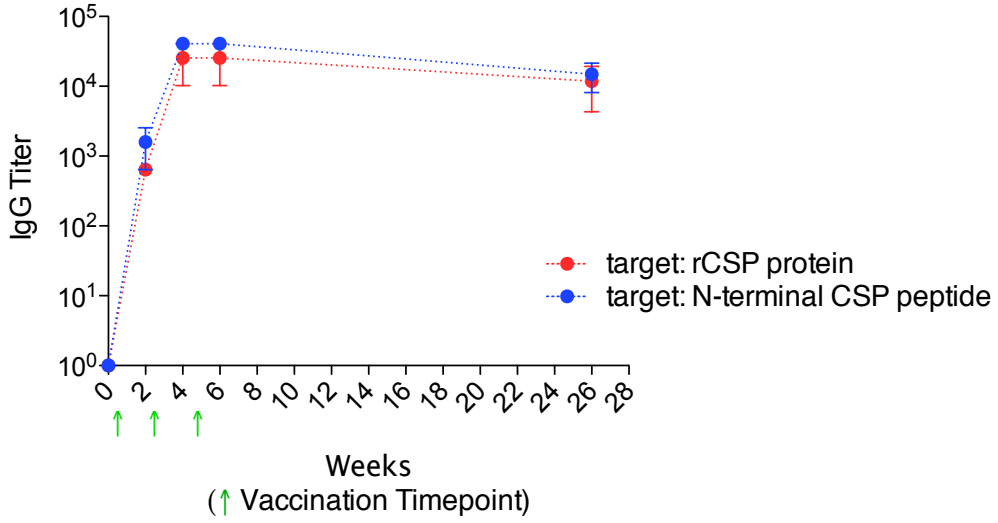

Figure 4.1. N-terminal CSP peptide-specific and recombinant CSP protein-reactive IgG titers achieved by immunization. N-terminal CSP peptide-conjugated Qβ VLP vaccine-elicited peptide titers were assessed in end-point dilution ELISAs for 5 immunized Balb/C mice, using N-terminal CSP peptide (blue) or recombinant CSP protein (red) as the target. Preimmune sera served as the negative control. Immunizations consisted of 5ug doses in 50% IFA. Mean and SEM are shown.

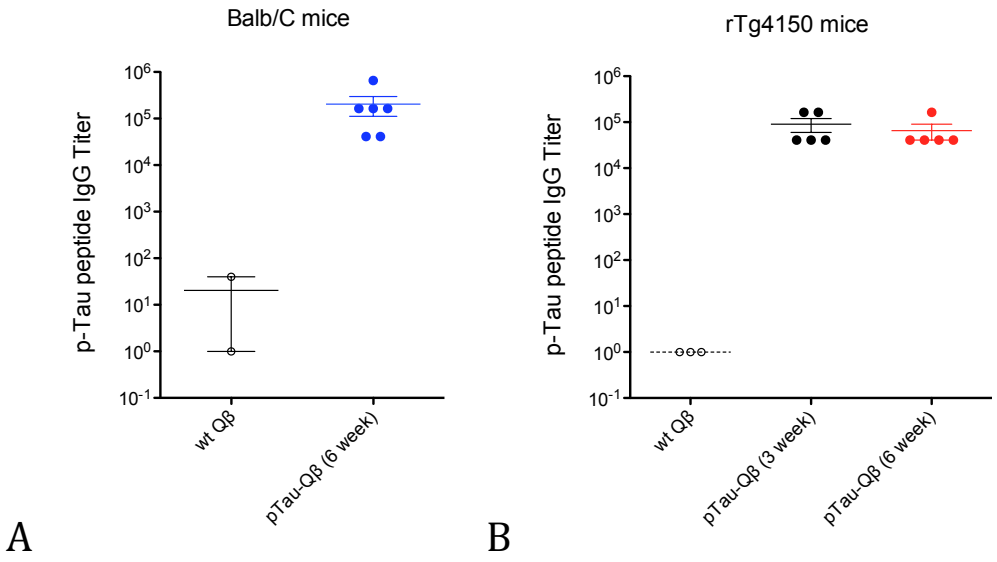

Figure 4.2. Phosphorylated-Tau peptide-specific IgG titers achieved by immunization. Phosphorylated-Tau peptide-conjugated Qβ VLP vaccine-elicited peptide titers were assessed in end-point dilution ELISAs for immunized wild-type Balb/C mice (A) and immunized rTg4150 mice that conditionally (Tet-off) express mutant human tau protein (B). Controls received wild-type Qβ VLPs, and all immunizations consisted of 5ug doses in 50% IFA. Mean and SEM are shown.

References

1. Romanowski, B., et al., *Sustained efficacy and immunogenicity of the human papillomavirus (HPV)-16/18 AS04-adjuvanted vaccine: analysis of a randomised placebo-controlled trial up to 6.4 years.* Lancet, 2009. **374**(9706): p. 1975-85.
2. Kao, J.H. and D.S. Chen, *Global control of hepatitis B virus infection.* The Lancet Infectious Diseases, 2002. **2**(7): p. 395-403.
3. Peabody, D.S., Manifold-Wheeler, B., Medford, A., Jordan, S. K., Caldeira, J. C., and Chackerian, B., *Immunogenic display of diverse peptides on virus-like particles of RNA phage MS2.* Journal of Molecular Biology, 2008. **380**(1): p. 252-63.
4. Caldeira, J.C., Medford, A., Kines, R. C., Lino, C. A., Schiller, J. T., Chackerian, B., and Peabody, D. S., *Immunogenic display of diverse peptides, including a broadly cross-type neutralizing human papillomavirus L2 epitope, on virus-like particles of the RNA bacteriophage PP7.* Vaccine, 2010. **28**(27): p. 4384-4393.
5. Chackerian, B., Rangel, M., Hunter, Z., and Peabody, D. S., *Virus and virus-like particle-based immunogens for Alzheimer's disease induce antibody responses against amyloid-beta without concomitant T cell responses.* Vaccine, 2006. **24**(37-39): p. 6321-31.
6. Chackerian, B., *Virus-like particles: flexible platforms for vaccine development.* Expert Rev Vaccines, 2007. **6**(3): p. 381-90.
7. Dintzis, R.Z., B. Vogelstein, and H.M. Dintzis, *Specific cellular stimulation in the primary immune response: experimental test of a quantized model.* Proc Natl Acad Sci U S A, 1982. **79**(3): p. 884-8.
8. Bachmann, M.F., et al., *The influence of antigen organization on B cell responsiveness.* Science, 1993. **262**(5138): p. 1448-1451.
9. Thyagarajan, R., N. Arunkumar, and W. Song, *Polyvalent antigens stabilize B cell antigen receptor surface signaling microdomains.* J Immunol, 2003. **170**(12): p. 6099-106.
10. Oliveira, G.A., et al., *Safety and enhanced immunogenicity of a hepatitis B core particle Plasmodium falciparum malaria vaccine formulated in adjuvant Montanide ISA 720 in a phase I trial.* Infect Immun, 2005. **73**(6): p. 3587-97.
11. Jennings, G.T. and M.F. Bachmann, *Immunodrugs: therapeutic VLP-based vaccines for chronic diseases.* Annu Rev Pharmacol Toxicol, 2009. **49**: p. 303-26.
12. Chackerian, B., D.R. Lowy, and J.T. Schiller, *Conjugation of a self-antigen to papillomavirus-like particles allows for efficient induction of protective autoantibodies.* Journal of Clinical Investigation, 2001. **108**(3): p. 415-23.
13. Bard, F., et al., *Epitope and isotype specificities of antibodies to beta -amyloid peptide for protection against Alzheimer's disease-like neuropathology.* Proc Natl Acad Sci U S A, 2003. **100**(4): p. 2023-8.
14. Apostolopoulos, V., et al., *Pilot phase III immunotherapy study in early-stage breast cancer patients using oxidized mannan-MUC1 [ISRCTN71711835].* Breast Cancer Res, 2006. **8**(3): p. R27.

15. Duff, C.J., et al., *Antibody-mediated disruption of the interaction between PCSK9 and the low-density lipoprotein receptor.* Biochem J, 2009. **419**(3): p. 577-584.
16. Coley, A.M., et al., *Rapid and precise epitope mapping of monoclonal antibodies against Plasmodium falciparum AMA1 by combined phage display of fragments and random peptides.* Protein Eng, 2001. **14**(9): p. 691-8.
17. Dormitzer, P.R., G. Grandi, and R. Rappuoli, *Structural vaccinology starts to deliver.* Nat Rev Microbiol, 2012. **10**(12): p. 807-13.
18. Grimm, S.K. and M.E. Ackerman, *Vaccine design: emerging concepts and renewed optimism.* Curr Opin Biotechnol, 2013. **24**(6): p. 1078-88.
19. Tonkin, M.L., et al., *Host cell invasion by apicomplexan parasites: insights from the co-structure of AMA1 with a RON2 peptide.* Science, 2011. **333**(6041): p. 463-7.
20. Kwon, H.J., et al., *Molecular basis for LDL receptor recognition by PCSK9.* Proceedings of the National Academy of Sciences, 2008. **105**(6): p. 1820-1825.
21. Collins, C.R., et al., *Fine mapping of an epitope recognized by an invasion-inhibitory monoclonal antibody on the malaria vaccine candidate apical membrane antigen 1.* J Biol Chem, 2007. **282**(10): p. 7431-41.
22. Bai, T., Becker, M., Gupta, A., Strike, P., Murphy, V. J., Anders, R. F., and Batchelor, A. H., *Structure of AMA1 from Plasmodium falciparum reveals a clustering of polymorphisms that surround a conserved hydrophobic pocket.* Proceedings of the National Academy of Sciences of the United States of America, 2005. **102**(36): p. 12736-12741.
23. Jegerlehner, A., et al., *A molecular assembly system that renders antigens of choice highly repetitive for induction of protective B cell responses.* Vaccine, 2002. **20**(25-26): p. 3104-12.
24. Jennings, G.T. and M.F. Bachmann, *The coming of age of virus-like particle vaccines.* Biol Chem, 2008. **389**(5): p. 521-36.
25. Hess, G.T., et al., *M13 bacteriophage display framework that allows sortase-mediated modification of surface-accessible phage proteins.* Bioconjug Chem, 2012. **23**(7): p. 1478-87.
26. Garufi, G., et al., *Sortase-conjugation generates a capsule vaccine that protects guinea pigs against Bacillus anthracis.* Vaccine, 2012. **30**(23): p. 3435-44.
27. Pallen, M.J., et al., *An embarrassment of sortases - a richness of substrates?* Trends Microbiol, 2001. **9**(3): p. 97-102.
28. Naik, M.T., et al., *Staphylococcus aureus Sortase A transpeptidase. Calcium promotes sorting signal binding by altering the mobility and structure of an active site loop.* J Biol Chem, 2006. **281**(3): p. 1817-26.
29. Connolly, K.M., et al., *Sortase from Staphylococcus aureus does not contain a thiolate-imidazolium ion pair in its active site.* J Biol Chem, 2003. **278**(36): p. 34061-5.
30. Peabody, D.S., *Translational repression by bacteriophage MS2 coat protein expressed from a plasmid. A system for genetic analysis of a protein-RNA interaction.* J Biol Chem, 1990. **265**(10): p. 5684-9.

31. Tumban, E., et al., *VLPs displaying a single L2 epitope induce broadly cross-neutralizing antibodies against human papillomavirus.* PLoS ONE. **7**(11): p. e49751.
32. Peabody, D.S., *Subunit fusion confers tolerance to peptide insertions in a virus coat protein.* Arch Biochem Biophys, 1997. **347**(1): p. 85-92.
33. Matthews, L.J., R. Davis, and G.P. Smith, *Immunogenically fit subunit vaccine components via epitope discovery from natural peptide libraries.* J Immunol, 2002. **169**(2): p. 837-46.
34. Irving, M.B., Craig, L., Menendez, A., Gangadhar, B. P., Montero, M., van Houten, N. E., and Scott, J. K., *Exploring peptide mimics for the production of antibodies against discontinuous protein epitopes.* Molecular Immunology, 2010. **47**(5): p. 1137-1148.
35. Geysen, H.M., S.J. Rodda, and T.J. Mason, *A priori delineation of a peptide which mimics a discontinuous antigenic determinant.* Mol Immunol, 1986. **23**(7): p. 709-15.
36. Beenhouwer, D.O., et al., *High affinity mimotope of the polysaccharide capsule of Cryptococcus neoformans identified from an evolutionary phage peptide library.* J Immunol, 2002. **169**(12): p. 6992-9.
37. Larralde, O.G., et al., *Identification of hepatitis A virus mimotopes by phage display, antigenicity and immunogenicity.* J Virol Methods, 2007. **140**(1-2): p. 49-58.
38. Knittelfelder, R., A.B. Riemer, and E. Jensen-Jarolim, *Mimotope vaccination--from allergy to cancer.* Expert Opin Biol Ther, 2009. **9**(4): p. 493-506.
39. Chackerian, B., Caldeira, J. C., Peabody, J., and Peabody, D. S., *Peptide Epitope Identification by Affinity Selection on Bacteriophage MS2 Virus-Like Particles.* Journal of Molecular Biology, 2011. **409**(2): p. 225-237.
40. Seidah, N.G., et al., *The secretory proprotein convertase neural apoptosis-regulated convertase 1 (NARC-1): Liver regeneration and neuronal differentiation.* Proceedings of the National Academy of Sciences, 2003. **100**(3): p. 928-933.
41. Abifadel, M., et al., *Mutations in PCSK9 cause autosomal dominant hypercholesterolemia.* Nature Genetics, 2003. **34**(2): p. 154-156.
42. Cohen, J.C., et al., *Sequence Variations in PCSK9, Low LDL, and Protection against Coronary Heart Disease.* New England Journal of Medicine, 2006. **354**(12): p. 1264-1272.
43. Zhao, Z., et al., *Molecular Characterization of Loss-of-Function Mutations in PCSK9 and Identification of a Compound Heterozygote.* The American Journal of Human Genetics, 2006. **79**(3): p. 514-523.
44. Piper, D.E., et al., *The Crystal Structure of PCSK9: A Regulator of Plasma LDL-Cholesterol.* Structure, 2007. **15**(5): p. 545-552.
45. Cunningham, D., et al., *Structural and biophysical studies of PCSK9 and its mutants linked to familial hypercholesterolemia.* Nat Struct Mol Biol, 2007. **14**(5): p. 413-419.
46. Qian, Y.-W., et al., *Secreted PCSK9 downregulates low density lipoprotein receptor through receptor-mediated endocytosis.* Journal of Lipid Research, 2007. **48**(7): p. 1488-1498.

47. Horton, J.D., J.L. Goldstein, and M.S. Brown, *SREBPs: activators of the complete program of cholesterol and fatty acid synthesis in the liver.* The Journal of Clinical Investigation, 2002. **109**(9): p. 1125-1131.
48. Rashid, S., et al., *Decreased plasma cholesterol and hypersensitivity to statins in mice lacking Pcsk9.* Proceedings of the National Academy of Sciences of the United States of America, 2005. **102**(15): p. 5374-5379.
49. Stein, E.A., et al., *Effect of a Monoclonal Antibody to PCSK9 on LDL Cholesterol.* New England Journal of Medicine, 2012. **366**(12): p. 1108-1118.
50. Chan, J.C.Y., et al., *A proprotein convertase subtilisin/kexin type 9 neutralizing antibody reduces serum cholesterol in mice and nonhuman primates.* Proceedings of the National Academy of Sciences, 2009. **106**(24): p. 9820-9825.
51. Hart, T.K., et al., *Preclinical efficacy and safety of pascolizumab (SB 240683): a humanized anti-interleukin-4 antibody with therapeutic potential in asthma.* Clinical & Experimental Immunology, 2002. **130**(1): p. 93-100.
52. Tobinai, K., et al., *Feasibility and pharmacokinetic study of a chimeric anti-CD20 monoclonal antibody (IDEC-C2B8, rituximab) in relapsed B-cell lymphoma.* Annals of Oncology, 1998. **9**(5): p. 527-534.
53. De Groot, A.S. and D.W. Scott, *Immunogenicity of protein therapeutics.* Trends in Immunology, 2007. **28**(11): p. 482-490.
54. Baert, F., et al., *Influence of Immunogenicity on the Long-Term Efficacy of Infliximab in Crohn's Disease.* New England Journal of Medicine, 2003. **348**(7): p. 601-608.
55. Suntharalingam, G., et al., *Cytokine Storm in a Phase 1 Trial of the Anti-CD28 Monoclonal Antibody TGN1412.* New England Journal of Medicine, 2006. **355**(10): p. 1018-1028.
56. Chackerian, B., D.R. Lowy, and J.T. Schiller, *Induction of autoantibodies to mouse CCR5 with recombinant papillomavirus particles.* Proceedings of the National Academy of Sciences, 1999. **96**: p. 2373-2378.
57. Chackerian, B., Lenz, P., Lowy, D. R., and Schiller, J. T., *Determinants of autoantibody induction by conjugated papillomavirus virus-like particles.* Journal of Immunology, 2002. **169**(11): p. 6120-6.
58. Chackerian, B., M.R. Durfee, and J.T. Schiller, *Virus-like display of a neo-self antigen reverses B cell anergy in a B cell receptor transgenic mouse model.* J Immunol, 2008. **180**(9): p. 5816-25.
59. Chackerian, B., et al., *Virus and virus-like particle-based immunogens for Alzheimer's disease induce antibody responses against amyloid-beta without concomitant T cell responses.* Vaccine, 2006. **24**(37-39): p. 6321-31.
60. Maxwell, K.N., E.A. Fisher, and J.L. Breslow, *Overexpression of PCSK9 accelerates the degradation of the LDLR in a post-endoplasmic reticulum compartment.* Proceedings of the National Academy of Sciences of the United States of America, 2005. **102**(6): p. 2069-2074.
61. Maxwell, K.N. and J.L. Breslow, *Adenoviral-mediated expression of Pcsk9 in mice results in a low-density lipoprotein receptor knockout phenotype.* Proceedings of the National Academy of Sciences of the United States of America, 2004. **101**(18): p. 7100-7105.

62. Jawien, J., P. Nastalek, and R. Korbut, *Mouse models of experimental atherosclerosis.* Journal of Physiology and Pharmacology, 2004. **55**(3): p. 503-517.
63. Rutledge, J.C., et al., *Lipoprotein Lipase Increases Lipoprotein Binding to the Artery Wall and Increases Endothelial Layer Permeability by Formation of Lipolysis Products.* Circulation Research, 1997. **80**(6): p. 819-828.
64. Cameron, J., et al., *Investigations on the evolutionary conservation of PCSK9 reveal a functionally important protrusion.* FEBS Journal, 2008. **275**(16): p. 4121-4133.
65. Stein, E.A. and F. Raal, *Reduction of Low-Density Lipoprotein Cholesterol by Monoclonal Antibody Inhibition of PCSK9.* Annual Review of Medicine. **65**(1): p. 417-431.
66. Harper, D.M., et al., *Sustained efficacy up to 4.5 years of a bivalent L1 virus-like particle vaccine against human papillomavirus types 16 and 18: follow-up from a randomised control trial.* Lancet, 2006. **367**(9518): p. 1247-55.
67. Richter, L.J., et al., *Production of hepatitis B surface antigen in transgenic plants for oral immunization.* Nat Biotechnol, 2000. **18**(11): p. 1167-71.
68. Rodriguez-Limas, W.A., K. Sekar, and K.E. Tyo, *Virus-like particles: the future of microbial factories and cell-free systems as platforms for vaccine development.* Curr Opin Biotechnol, 2013. **24**(6): p. 1089-93.
69. Ferrieres, G., et al., *Affinity for the cognate monoclonal antibody of synthetic peptides derived from selection by phage display. Role of sequences flanking thebinding motif.* Eur J Biochem, 2000. **267**(6): p. 1819-29.
70. Mota, M.M., et al., *Migration of Plasmodium sporozoites through cells before infection.* Science, 2001. **291**(5501): p. 141-4.
71. Richard, D., et al., *Interaction between Plasmodium falciparum Apical Membrane Antigen 1 and the Rhoptry Neck Protein Complex Defines a Key Step in the Erythrocyte Invasion Process of Malaria Parasites.* Journal of Biological Chemistry, 2010. **285**(19): p. 14815-14822.
72. Miller, L.H., et al., *The pathogenic basis of malaria.* Nature, 2002. **415**(6872): p. 673-9.
73. Richards, J.S., et al., *Identification and prioritization of merozoite antigens as targets of protective human immunity to Plasmodium falciparum malaria for vaccine and biomarker development.* J Immunol, 2013. **191**(2): p. 795-809.
74. Pizarro, J.C., Normand, B. V., Chesne-Seck, M., Collins, C. R., Withers-Martinez, C., Hackett, F., Blackman, M. J., Faber, B. W., Remarque, E. J., Kocken, C. H. M., Thomas, A. W., and Bentley, G. A., *Crystal Structure of the Malaria Vaccine Candidate Apical Membrane Antigen 1.* Science, 2005. **308**(5720): p. 408-411.
75. Chesne-Seck, M.L., et al., *Structural comparison of apical membrane antigen 1 orthologues and paralogues in apicomplexan parasites.* Mol Biochem Parasitol, 2005. **144**(1): p. 55-67.
76. Weiss, G.E., et al., *The Plasmodium falciparum-specific human memory B cell compartment expands gradually with repeated malaria infections.* PLoS Pathog, 2010. **6**(5): p. e1000912.
77. Kocken, C.H., et al., *High-level expression of the malaria blood-stage vaccine candidate Plasmodium falciparum apical membrane antigen 1 and induction of*

antibodies that inhibit erythrocyte invasion. Infect Immun, 2002. **70**(8): p. 4471-6.
78. Hodder, A.N., P.E. Crewther, and R.F. Anders, *Specificity of the protective antibody response to apical membrane antigen 1.* Infect Immun, 2001. **69**(5): p. 3286-94.
79. Thomas, A.W., et al., *High prevalence of natural antibodies against Plasmodium falciparum 83-kilodalton apical membrane antigen (PF83/AMA-1) as detected by capture-enzyme-linked immunosorbent assay using full-length baculovirus recombinant PF83/AMA-1.* Am J Trop Med Hyg, 1994. **51**(6): p. 730-40.
80. Malkin, E.M., et al., *Phase 1 clinical trial of apical membrane antigen 1: an asexual blood-stage vaccine for Plasmodium falciparum malaria.* Infect Immun, 2005. **73**(6): p. 3677-85.
81. Thera, M.A., et al., *Safety and immunogenicity of an AMA-1 malaria vaccine in Malian adults: results of a phase 1 randomized controlled trial.* PLoS ONE, 2010. **3**(1): p. e1465.
82. Sok, D., B. Moldt, and D.R. Burton, *SnapShot: broadly neutralizing antibodies.* Cell, 2013. **155**(3): p. 728-728 e1.
83. Dutta, S., et al., *Alanine mutagenesis of the primary antigenic escape residue cluster, c1, of apical membrane antigen 1.* Infect Immun, 2010. **78**(2): p. 661-71.
84. Laurens, M.B., et al., *Extended safety, immunogenicity and efficacy of a blood-stage malaria vaccine in malian children: 24-month follow-up of a randomized, double-blinded phase 2 trial.* PLoS ONE, 2013. **8**(11): p. e79323.
85. Dutta, S., et al., *Overcoming antigenic diversity by enhancing the immunogenicity of conserved epitopes on the malaria vaccine candidate apical membrane antigen-1.* PLoS Pathog, 2013. **9**(12): p. e1003840.
86. Bai, T., et al., *Structure of AMA1 from Plasmodium falciparum reveals a clustering of polymorphisms that surround a conserved hydrophobic pocket.* Proc Natl Acad Sci U S A, 2005. **102**(36): p. 12736-41.
87. Coley, A.M., et al., *Structure of the malaria antigen AMA1 in complex with a growth-inhibitory antibody.* PLoS Pathog, 2007. **3**(9): p. 1308-19.
88. Narum, D.L. and A.W. Thomas, *Differential localization of full-length and processed forms of PF83/AMA-1 an apical membrane antigen of Plasmodium falciparum merozoites.* Mol Biochem Parasitol, 1994. **67**(1): p. 59-68.
89. Anders, R.F., et al., *Immunisation with recombinant AMA-1 protects mice against infection with Plasmodium chabaudi.* Vaccine, 1998. **16**(2-3): p. 240-7.
90. Kocken, C.H., et al., *Precise timing of expression of a Plasmodium falciparum-derived transgene in Plasmodium berghei is a critical determinant of subsequent subcellular localization.* J Biol Chem, 1998. **273**(24): p. 15119-24.
91. Collins, C.R., Withers-Martinez, C., Hackett, F., and Blackman, M. J., *An Inhibitory Antibody Blocks Interactions between Components of the Malarial Invasion Machinery.* PLoS Pathog, 2009. **5**(1): p. e1000273.
92. Sabo, J.K., et al., *Mimotopes of apical membrane antigen 1: Structures of phage-derived peptides recognized by the inhibitory monoclonal antibody 4G2dc1 and design of a more active analogue.* Infect Immun, 2007. **75**(1): p. 61-73.

93. Mueller, M.S., et al., *Induction of parasite growth-inhibitory antibodies by a virosomal formulation of a peptidomimetic of loop I from domain III of Plasmodium falciparum apical membrane antigen 1.* Infect Immun, 2003. **71**(8): p. 4749-58.
94. Hill, A.V., *Pre-erythrocytic malaria vaccines: towards greater efficacy.* Nat Rev Immunol, 2006. **6**(1): p. 21-32.
95. Kim, Y., et al., *Immune epitope database analysis resource.* Nucleic Acids Res, 2012. **40**(Web Server issue): p. W525-30.
96. Crooks, G.E., et al., *WebLogo: a sequence logo generator.* Genome Res, 2004. **14**(6): p. 1188-90.
97. Olszewska, W., O.E. Obeid, and M.W. Steward, *Protection against measles virus-induced encephalitis by anti-mimotope antibodies: the role of antibody affinity.* Virology, 2000. **272**(1): p. 98-105.
98. Irving, M.B., O. Pan, and J.K. Scott, *Random-peptide libraries and antigen-fragment libraries for epitope mapping and the development of vaccines and diagnostics.* Curr Opin Chem Biol, 2001. **5**(3): p. 314-24.
99. Menard, R., et al., *Looking under the skin: the first steps in malarial infection and immunity.* Nat Rev Microbiol, 2013. **11**(10): p. 701-12.
100. Kumar, K.A., et al., *The circumsporozoite protein is an immunodominant protective antigen in irradiated sporozoites.* Nature, 2006. **444**(7121): p. 937-40.
101. Reece, W.H., et al., *A CD4(+) T-cell immune response to a conserved epitope in the circumsporozoite protein correlates with protection from natural Plasmodium falciparum infection and disease.* Nat Med, 2004. **10**(4): p. 406-10.
102. Bongfen, S.E., et al., *The N-terminal domain of Plasmodium falciparum circumsporozoite protein represents a target of protective immunity.* Vaccine, 2009. **27**(2): p. 328-35.
103. Zeeshan, M., et al., *Genetic variation in the Plasmodium falciparum circumsporozoite protein in India and its relevance to RTS,S malaria vaccine.* PLoS ONE, 2012. **7**(8): p. e43430.
104. Coppi, A., et al., *The Plasmodium circumsporozoite protein is proteolytically processed during cell invasion.* J Exp Med, 2005. **201**(1): p. 27-33.
105. Porter, M.D., et al., *Transgenic parasites stably expressing full-length Plasmodium falciparum circumsporozoite protein as a model for vaccine down-selection in mice using sterile protection as an endpoint.* Clin Vaccine Immunol, 2013. **20**(6): p. 803-10.
106. Tewari, R., et al., *Function of region I and II adhesive motifs of Plasmodium falciparum circumsporozoite protein in sporozoite motility and infectivity.* J Biol Chem, 2002. **277**(49): p. 47613-8.
107. Clavaguera, F., et al., *Transmission and spreading of tauopathy in transgenic mouse brain.* Nat Cell Biol, 2009. **11**(7): p. 909-13.
108. Saman, S., et al., *Exosome-associated tau is secreted in tauopathy models and is selectively phosphorylated in cerebrospinal fluid in early Alzheimer disease.* J Biol Chem, 2012. **287**(6): p. 3842-9.

109. Cushman, M., et al., *Prion-like disorders: blurring the divide between transmissibility and infectivity.* J Cell Sci, 2010. **123**(Pt 8): p. 1191-201.
110. Perez, P.D., et al., *In vivo functional brain mapping in a conditional mouse model of human tauopathy (tau(P301L)) reveals reduced neural activity in memory formation structures.* Mol Neurodegener, 2013. **8**: p. 9.